Creation of a novel class of potent and selective MutT Homolog 1 (MTH1) inhibitors using fragment-based screening and structure-based drug design

Fredrik Rahm,[#§] Jenny Viklund,[#] Lionel Trésaugues,[#] Manuel Ellermann,[†] Anja Giese,[†] Ulrika Ericsson,[#] Rickard Forsblom,[#] Tobias Ginman,[#] Judith Günther,[†] Kenth Hallberg,[#‡] Johan Lindström,[#] Lars Boukharta Persson,[#] Camilla Silvander,[#] Antoine Talagas,[#] Laura Díaz-Sáez,[‖,$] Oleg Fedorov,[‖,$] Kilian V. M. Huber,[‖,$] Ioanna Panagakou,[‖,$] Paulina Siejka,[‖,$] Mátyás Gorjánácz,[†] Marcus Bauser,[†] and Martin Andersson [#]*

[#]Sprint Bioscience AB, Novum, 141 57 Huddinge, Sweden

[†] Bayer AG, Muellerstrasse 178, 133 53 Berlin, Germany

[‖]Structural Genomics Consortium, Nuffield Department of Medicine, University of Oxford, Oxford, United Kingdom, OX3 7DQ

[$]Target Discovery Institute, Nuffield Department of Medicine, University of Oxford, Oxford, United Kingdom, OX3 7FZ

KEYWORDS: MTH1, fragment-based drug discovery, fragment growing, structure-based drug discovery, target validation, BAY-707

ABSTRACT

Recent literature has both suggested and questioned MTH1 as a novel cancer target. BAY-707 was just published as a target validation small molecule probe for assessing the effects of pharmacological inhibition of MTH1 on tumor cell survival, both *in vitro* and *in vivo*.[1] In this report, we describe the medicinal chemistry program creating BAY-707, where fragment-based methods were used to develop a series of highly potent and selective MTH1 inhibitors. Using structure-based drug design and rational medicinal chemistry approaches, the potency was increased over 10.000 times from the fragment starting point, while maintaining high ligand efficiency and drug-like properties.

INTRODUCTION

One prominent feature of cancer is the increase in reactive oxygen species (ROS) in cancer cells as compared to normal cells.[2] ROS are generated during cell metabolism and are highly reactive towards most biological macromolecules such as nucleic acids and proteins.[3] Hence, cancer cells have a higher dependency than normal cells on various ROS-related defense mechanisms, and consequently, such pathways have been suggested as potential targets for cancer treatments.[4]

The nucleotide pool is also subject to oxidative damage by ROS, with the main oxidation products being 8-oxo-7,8-dihydro-2'-deoxyguanosine (8-oxo-dG) and its corresponding nucleotides.[5] Oxidized nucleotide triphosphates (such as 8-oxo-dGTP) are mutagenic and cytotoxic when incorporated into DNA.[6] To clear the nucleotide pool of such damaged nucleotides, cells are equipped with enzymes, such as members of the NUDIX family (NUcleoside DIphosphate linked to another moiety X).[7] Recent studies have suggested a dependency of cancer cells to a particular enzyme of this family; Nudix hydrolase 1 (NUDT1) - also called MutT Homolog1 (MTH1), which is upregulated in several cancer forms.[8] MTH1 catalyzes the hydrolysis of 8-oxo-dGTP and scarcer oxidized nucleotides triphosphates to their monophosphate counterparts, thus preventing their incorporation into DNA. The 8-oxo-dGMP product is further hydrolyzed to 8-oxo-dG and excreted from the cell.[9]

The first discoveries relating MTH1 to a role in cancer biology was published in 2011, in a study that identified MTH1 as one of the genes induced by RAS overexpression.[10] Given its role in nucleotide pool sanitization and ROS stress defense, further studies by the same authors showed that MTH1 knockdown inhibits RAS-driven tumor cell growth *in vitro* and *in vivo*.[11] More data was published during 2014 lending further support to the hypothesis that MTH1 has a role in

prevention of DNA damage and cancer cell survival. It was shown that a phenotypic screening hit, SCH51344 that inhibits the non-adherent growth of cancer cells, is an MTH1 inhibitor.[12] (*S*)-Crizotinib was also identified in this screen as a more selective MTH1 inhibitor, and it was shown that these compounds induce DNA damage and inhibit tumor cell growth both *in vitro* and *in vivo*. In a third study, pharmacological target validation also looked promising, both *in vitro* and *in vivo*, using the novel MTH1 inhibitor TH588.[8]

The first crystal structure of MTH1 became available in the PDB in 2011.[13,14] The global interest in this potential cancer target is revealed by the large number of structures of complexes which have been released since then. More than 20 complex structures with either nucleotide analogues or small molecule inhibitors have been published: the first one being with 8-oxo-GMP, the product formed by hydrolysis of the main substrate, 8-oxo-dGTP.[15,16] These ligands are all competitive binders,[8,12,17] and they share common binding motifs with the purine ring of the substrate, including one or more hydrogen-bonds to the "key Asp119-Asp120 recognition element".[16] Even though the ligand interactions to these aspartates appear to be crucial, the number and positions of the atoms involved in hydrogen-bonding can vary significantly (Figure 1).

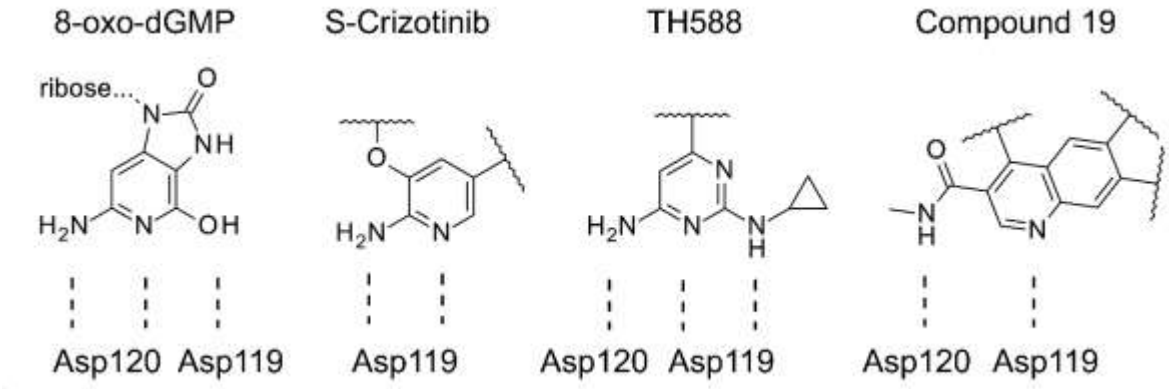

Figure 1. Representations of the key interactions of selected inhibitors of MTH1 (the corresponding PDB ID is shown in parenthesis), with varying hydrogen bonding patterns to the Asp119-Asp120 recognition element (dotted lines): 8-oxo-GMP (3ZR0)[18], (*S*)-Crizotinib (4C9X)[12], TH588 (4N1U)[8], AZ Compound 19 (5ANV)[17].

In 2016, reports started to appear that questioned the role of MTH1 in cancer cell survival.[17,19] In one study, proteomic profiling was used to conclude that the proteome-wide fingerprints of cells exposed to some of the pharmacological tools described in the 2014 studies did not resemble the proteomic fingerprints of other DNA-damage inducing agents or other MTH1 inhibitors, indicating that the observed effects of these compounds might be due to off-target effects.[20] These opposing results compared to the previous reports from 2014 emphasize the importance of using high quality, orthogonal probes for target validation.[21–24]

Since none of the above publications from 2016 reported results from *in vivo* studies, the hypothesis that MTH1 inhibition affects tumor growth *in vivo* could not be ruled out. To test this suggestion, a novel MTH1 inhibitor (BAY-707) was recently used to evaluate the effects of pharmacological target inhibition in a broad array of model systems, both *in vitro* and *in vivo*,

confirming the de-validation results from 2016[1]. This report describes the medicinal chemistry program that created BAY-707, using fragment-based drug discovery methods.

CHEMISTRY

Compounds described in this report are based on 7-azaindole, 7-azaindazole or 7-azabenzimidazole core structures, substituted in the 4-position and, in the first, optionally in the 2-position. The compounds were made by following a few general synthetic routes, as illustrated by Method A and Method B outlined in Scheme 1 below. Depending on the nature of the substituent in the 4-position, either the Suzuki-Miyaura[25] cross-coupling reaction, the Buchwald-Hartwig[26,27] cross-coupling reaction or direct nucleophilic aromatic substitution was used to introduce this substituent. To enable further functionalization in the 2-position of the core structure, suitable handles were introduced by standard deprotonation procedures followed by reaction with an appropriate electrophile. Some compounds were synthesized by combining one of these routes with additional standard functional group transformations. Full details regarding the synthesis of all compounds can be found in the experimental section.

General method A[a]

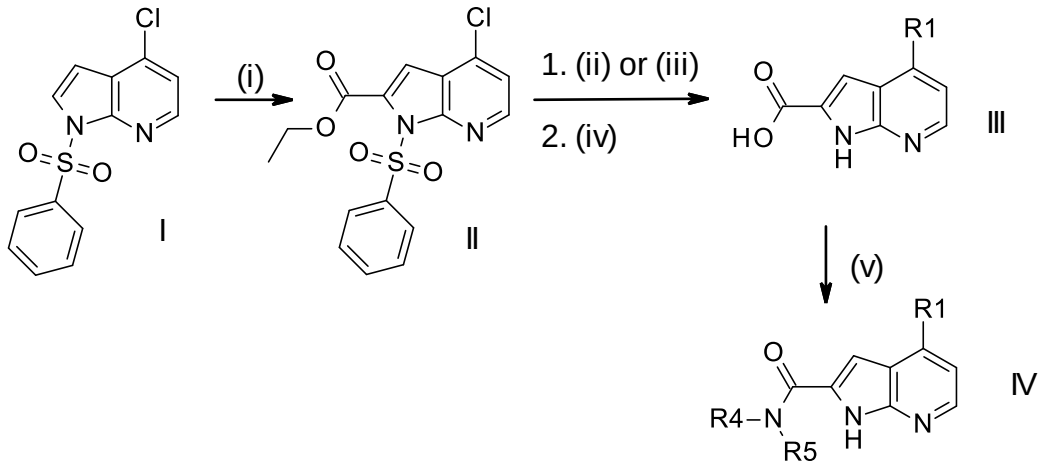

General method B[a]

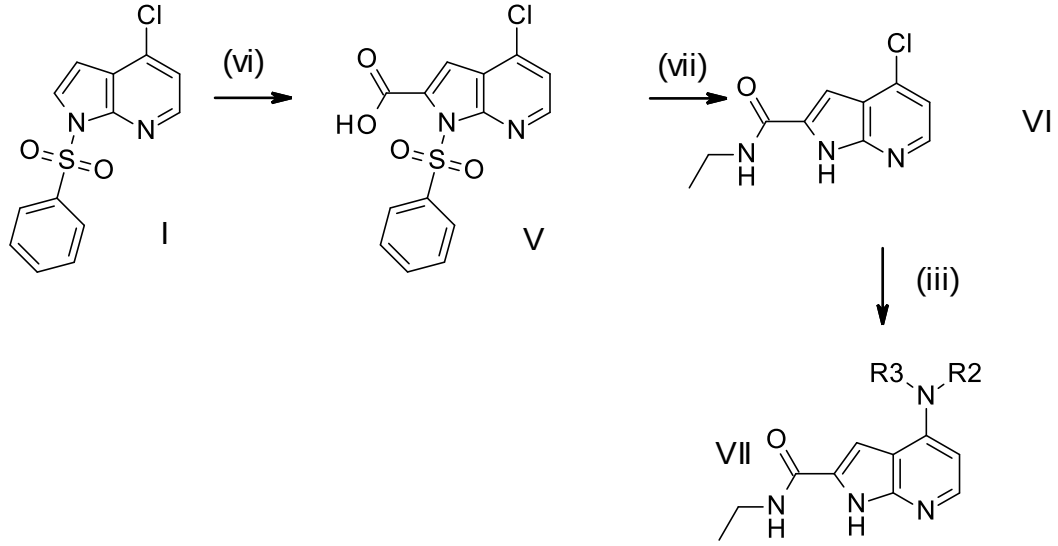

Scheme 1. [a]Reagents and conditions: (i) LDA, EtOCOCl, 2-MeTHF, -78 °C to rt; (ii) R1=aryl: boronic acid reagent, Pd(amphos)Cl_2, K_2CO_3, MeCN:H_2O, 120 °C; (iii) R^1=-NR^2R^3: cyclic secondary amine, NMP, 160 °C; (iv) LiOH·H_2O, THF:MeOH:H_2O, 50 °C; (v) (a) $SOCl_2$, 80 °C, (b) R^4R^5NH, THF, 0 °C to rt; (vi) LDA, 2-MeTHF, CO_2, -78 °C to rt; (vii) (a) $SOCl_2$, 80 °C, (b) $EtNH_2$, THF, 0 °C to rt.

RESULTS AND DISCUSSION

Primary screening was performed using a fluorescence-based thermal shift assay (TSA) to screen a library of 723 fragments at a compound concentration of 1 mM. The TSA monitors ligand effects on temperature-dependent protein unfolding, where ligand binding would lead to a positive T_m shift, as compared to the T_m of the apo-protein control. Hits were determined based on a change in T_m of MTH1 equal to or greater than three standard deviations of the mean of the T_m for the reference. Consequently, fragments with a ΔT_m value of more than +1.0°C in both duplicates were defined as hits. Applying this threshold, 166 fragments were identified that significantly increased the thermal melting point of MTH1, with ΔT_m values ranging from 1.0 to 11.8°C. Such high hit-rate (23%) is usually indicative of a druggable active site.[28]

Dose-response experiments were performed to verify the stabilization of MTH1 for the most promising hits from the single-point screening. The fragment concentrations were varied from 62.5 to 1000 μM and it was determined that the shift in ΔT_m was dose-dependent for 48 of 49 tested initial hit fragments. One of the screening hits was a 7-azaindole compound, fragment hit **1**, with a single point ΔT_m of 3.9 °C at 1 mM (Figure 2). 1:1 binding was verified with ITC, with a K_d of 49.5 μM (Figure S1). The azaindole was neither the most potent nor the most ligand efficient fragment among the verified hits. Still, it was selected to be explored considering its tractability from several other important perspectives: the azaindole core was providing synthetically reasonable attachment points to grow the fragment into interesting parts of the protein. Also, we were intentionally avoiding mainly lipophilic fragments containing a basic amine.[29] And last, all fragments containing the same aspartate-binding amino-pyrimidine and amino-pyridine cores as the reference compounds TH588 and S-Crizotinib were deselected, to ensure the creation of a novel and orthogonal series (Figure 1).

The fragment hit **1** was co-crystallized with human MTH1 protein and the 7-azaindole core was shown to make hydrogen bonds to both residues in the key recognition element mentioned above: the acceptor is interacting with Asp119 and the donor is interacting with Asp120 (Figure 2a). The 7-azaindole core is sandwiched through pi-stacking interactions between aromatic moieties of both Phe72 and Trp117 (Figure. 2b and 2c). The ester motif of **1** occupies the same area as the ribose part of the product, indicating the 4-position of the 7-azaindole ring system as an interesting starting point for growing the fragment hit into a larger molecule, aiming to increase binding affinity. Analysis of the crystal structure of **1** in complex with MTH1 revealed the existence of a minor pocket nearby Asp120, which we hypothesized could be targeted from the 2-position of the 7-azaindole core structure (pocket 1, Figure 2b).

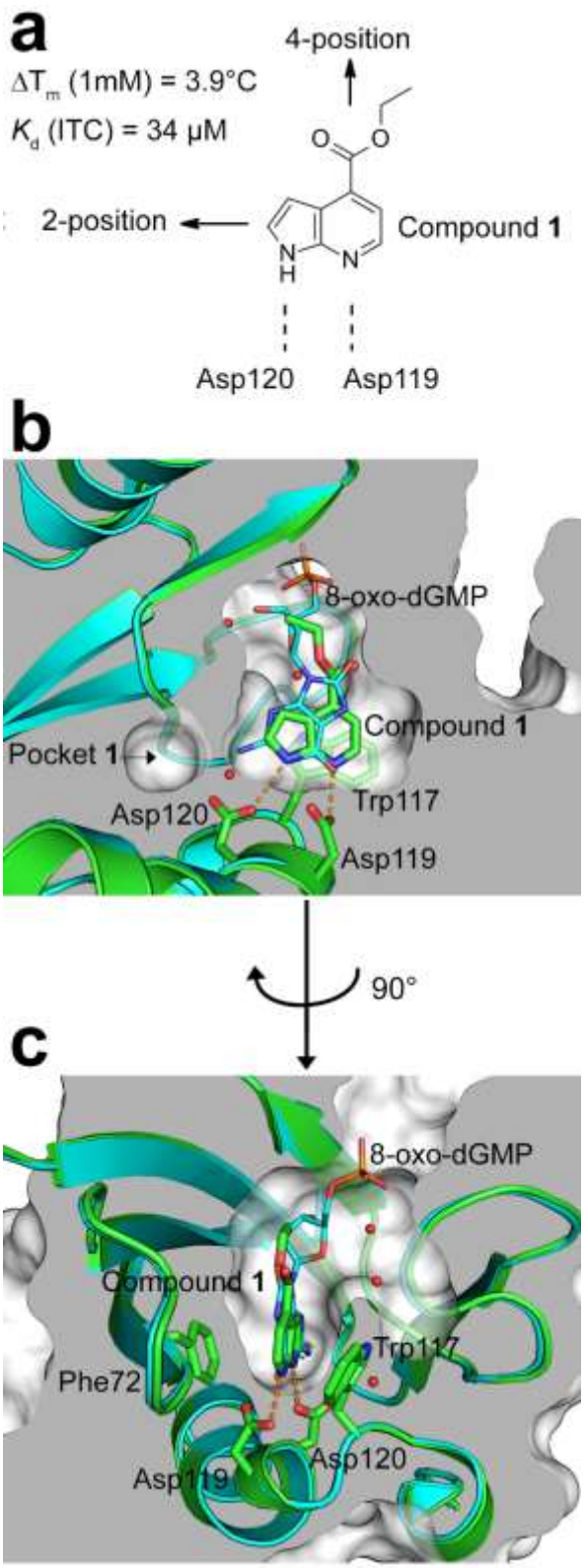
a
ΔT$_m$ (1mM) = 3.9°C
K_d (ITC) = 34 μM
4-position
2-position
Compound 1
Asp120
Asp119
b
8-oxo-dGMP
Compound 1
Pocket 1
Asp120
Trp117
Asp119
90°
c
8-oxo-dGMP
Compound 1
Trp117
Phe72
Asp120
Asp119

Figure 2. (a) The 2D structure of fragment hit **1.** Vectors from the 2- and 4-positions illustrate the attachment points for synthetic expansions presented in this work. (b) and (c) Overlay of complex between MTH1 and **1** (green, PDB ID: 6F20) and complex between MTH1 and 8-oxo-dGMP (cyan, PDB ID: 3ZR0). Side-chains of Phe72, Trp117, Asp119 and Asp120 in the structure of MTH1-**1** complex are shown as sticks with their carbon atoms colored green. Water molecules present in the inhibitor binding site of MTH1-**1** complex are shown as red spheres. 8-oxo-dGMP is displayed as thin sticks, with its carbon atoms colored cyan. The ester motif occupies the same area as the ribose of 8-oxo-dGMP, and we refer to this area as the ribose pocket. Clipped molecular surface of MTH1 is shown in the MTH1-Compound 1 complex structure. Figure 2 (c) is rotated 90 degrees as compared to figure 2 (b).

With the crystal structure of **1** in hand, our first approach for improving the fragment was to investigate close analogues in our in-house compound collection. Based on the crystal structure, docking studies were performed, and two compounds (**2** and **3**, Table 2) both with a substituent in the 4-position of the 7-azaindole core, were predicted to maintain the binding mode of **1**. TSA data showed an increase in melting temperature for both compounds, suggesting an increased binding affinity as compared to compound **1** (Table 1). Encouraged by these data, compound **4**, with a more lipophilic group in the 4-position, was synthesized and tested together with compounds **1**, **2** and **3** in a biochemical MTH1 inhibition assay. All compounds showed an increased potency as compared to **1** with at most a 5-fold increase in potency for **4**, while maintaining a high ligand efficiency (LE)[30] (Table 1).

Next, we set out to explore whether pocket 1 (Figure 2b) could fit a substituent in the 2-position of the 7-azaindole core. By visual inspection of the pocket, we reasoned that compound **5** was

the only representative from our in-house collection with a substituent (amide) that was small enough to have a chance to fit into this minor pocket. It was encouraging to see that the amide in the 2-position increased biochemical potency 20 times as compared to the matched pair compound **3.** In addition, compound **5** maintained a high LE, high solubility and even lower lipophilicity (Table 1), indicating that exploring the 2-position would be an interesting option for optimization.

Table 1. Biophysical, biochemical and physicochemical data of fragment hit **1** and close analogues

	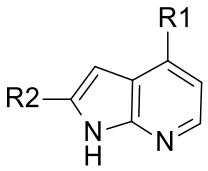		**TSA**	**Potency**		**Physicochemical properties**		
Compound	R1=	R2=	ΔT_m (°C)	Biochemical IC_{50} (μM)	LE	MW (Da)	clogP [b]	Solubility in buffer (mM)[c]
1	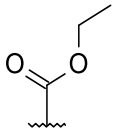	H	3.9	9.9	0.49	190.2	1.8	2
2	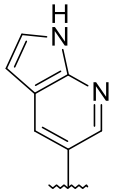	H	7.9	2.5	0.42	234.3	2.2	0.5
3	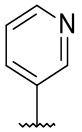	H	8.2	3.7	0.49	195.2	1.6	2
4	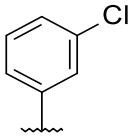	H	n.d. [a]	1.9	0.49	228.7	3.5	0.25
5	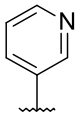	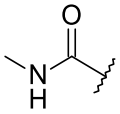	14.4	0.2	0.48	252.3	0.3	1

a) n.d. not determined

b) cLogP was calculated using the ChemAxon Partitioning Plugin v16.10.24

c) Solubility was estimated by visual inspection after dilution of the DMSO stock solution in buffer. The compounds were diluted at least 1/100, to give a final DMSO concentration not higher than 1 %.

Encouraged by the large potency gain from the amide of compound **5**, we synthesized a small set of five additional amide-containing compounds to further investigate the 2-position of the 7-azaindole core (**6-10**, Table 2). To generate matched-pair compounds with a balanced lipophilicity[31], m-chlorophenyl (as used in **4**) was chosen as substituent in the 4-position.

The crystal structure of the ethyl amide analogue **7** was solved in complex with MTH1, to understand the potency increase owing to the amide substituent in the 2-position. While the 7-azaindole core remains in the same position as seen for the fragment hit **1**, the amide makes two additional hydrogen bonds to the protein; the donor is interacting with Asp120, and the carbonyl acceptor is interacting with the backbone nitrogen of Gly34. In contrast to the crystal structure of **1**, Asn33 has moved into a different conformation, and is now replaced by the amide carbonyl (Figure 3). A similar interaction pattern, with a reversed amide substituent, was later published by others (Figure 1, AZ Compound 19).[17]

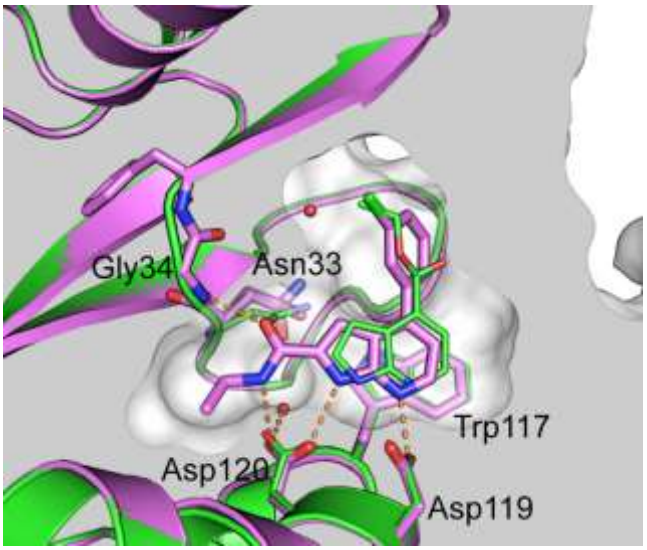

Figure 3. Crystal structure of **7**, showing that the 7-azaindole core remains in the same position as the fragment hit **1**. MTH1-**1** and MTH1-**7** complexes are colored green and violet respectively.

Residues interacting with the compounds, and compound themselves, are shown as thin (complex with **1**) or thick (complex with **7**) sticks with their carbon atoms colored following the same code as the secondary structure elements. Water molecules present in the binding-site of MTH1-**7** complex are shown as red spheres. Hydrogen bonds are displayed as orange dashes. Clipped molecular surface of MTH1 is shown in the MTH1-**7** complex structure (PDB ID: 6F1X).

From a computational chemistry perspective, it is interesting to note that neither the binding mode of **7**, nor any of its analogues, could be predicted correctly via docking studies, using any of the crystal structures available at that time (4C9X, 4C9W, 3ZR0, 3ZR1, 3Q93, 4N1T, 4N1U, Compound **1**). In all but one of these structures, the carbonyl of the flexible residue Asn33 is occupying the same position as the carbonyl of the amide of **7**. The only exception is 4CX9, where Asn33 occupies a similar position as in the MTH1-**7** complex. However, even when modifying the protonation states of the 4C9X aspartates to accommodate the hydrogen bonding pattern of **7**, the binding mode of the amide could still not be predicted correctly. We believe this is an interesting example of how computational selection methods of new compounds should be complemented by visual inspection of the crystal structures, to take advantage of the intuition of experienced medicinal chemists when doing structure-based design. In retrospect, however, we did try induced fit docking, allowing for the active site residues to be flexible, and with this more time-consuming protocol, the correct amide binding mode could indeed be predicted correctly.

In combination with the crystal structure of **7**, the small set of five amide-containing compounds generated distinct knowledge for the structure activity relationships (SAR) in 2-position: the importance of the hydrogen bond interaction with Asp120 is clearly seen in the severe drop in potency for the tertiary amide of **8**, lacking the donor. The equally severe drop in potency seen for the primary amide of **9**, shows the importance of filling the remaining part of pocket 1 with a

small alkyl substituent, which is then surrounded by the hydrophobic residues Leu11, Leu20, Met116 and Phe124. Thus, only secondary amides (**6**, **7**, and **10**) were well tolerated and resulted in compounds with low nM potencies and maintained LE (Table 2).

To further explore pocket 1, and particularly to investigate whether more diverse types of substituents other than amides were allowed in the 2-position, four additional matched-paired compounds were synthesized (Table 2). Attempts to gain potency by either simply filling the pocket with a methyl group (**11**) or by attempting to make polar interactions with the protein, as predicted by docking studies, were unsuccessful. Both compounds **12** and **13** contain other types of acceptors, aiming to mimic the amide carbonyl hydrogen bond to the backbone of Gly34. However, both the nitrile and the oxazole rather reduced potency, as compared to the matched pair compound **4**, without a substituent in the 2-position. Compound **14**, with a methylene hydroxyl substituent, was predicted by the docking studies to be able to either interact either as an acceptor to Gly34, or as a donor to Asp120. However, despite both of these hydrogen-bonding possibilities, **14** was merely equally potent as the matched pair compound **4**. To summarize to optimization efforts in the 2-position, the secondary amide analogues **6**, **7** and **10** were considered the most promising compounds so far, with low nM biochemical potency and high solubility.

Table 2. Biochemical potency and physicochemical properties for variations in 2-position.

	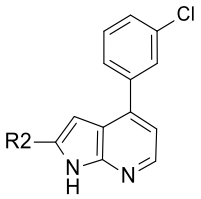	**Potency**		**Physicochemical properties**		
Compound	R2	Biochemical IC_{50} (μM)	LE	clogP	MW	Solubility in buffer (mM)
6	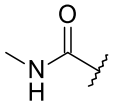	0.012	0.54	2.1	285.7	0.25
7	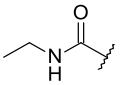	0.020	0.5	2.5	299.8	0.25
8	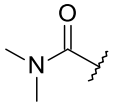	2.7	0.36	2.4	299.8	0.25
9	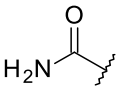	5.8	0.41	1.9	271.7	0.1
10	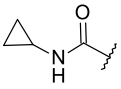	0.010	0.49	2.5	311.8	0.1
11		> 10		3.5	242.7	0.05
12	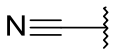	5.6	0.42	3.1	253.7	0.25
13	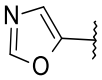	>10		2.6	295.7	0.05
14		1.4	0.44	2.4	258.7	0.01

Since our main objective was the development of both potent and highly selective MTH1 inhibitors, we wanted to assess the kinome selectivity profile already at this early stage of the program. We were especially concerned by the presence of the 7-azaindole core in our series, since this substructure is commonly seen as a hinge binding motif in kinase inhibitors.[32] Consequently, we assessed the kinome selectivity profile of **10**, as a representative structure of the azaindole series. Aiming for a selectivity window of at least 1000 times, compound **10** was tested in single point at 1 μM in a 97-member kinase panel [DiscoverX's scanEDGE™ Kinase Assay Panel]. It was encouraging to see that the compound did not hit any of the included kinases at significant levels [S-score = 0, Supporting information].

After the 2-position had been explored, we decided to continue the optimization work using the substituent in the 4-position, aiming to explore the ribose pocket further (Figure 2). A sitemap analysis using the crystal structure of MTH1-**7** proposed that this area would favor quite bulky, lipophilic substituents, possibly in combination with a donor to interact with any of the backbone carbonyls of Thr8, Phe27 or Gly34 (Figure S2, Supporting information). Consequently, we aimed to introduce larger lipophilic substituents with high 3D character, still retaining rigidity, in hope of improving potency by filling the ribose pocket more optimally. In addition, increasing the fraction of sp3 carbons is a general strategy to improve vital drug properties, such as metabolic stability, solubility and selectivity.[33,34]

A new set of compounds (**15 - 19**) with cyclic amines in the 4-position were selected for synthesis based on docking studies and availability of starting materials. We were intentionally avoiding additional donors to maintain high permeability.[35] Compound **16**, with a 2-phenylpyrrolidine in the 4-position, resulted in the highest increase of potency and LE (Table 3). The structure of the complex between **16** and MTH1 showed a maintained binding mode of the

7-azaindole core, and the bulky phenyl tightly occupying the pocket between the lipophilic residues Tyr7, Leu9 and Met81 (Figure 4). The most potent compounds **15** and **16**, together with the previous representative compound **10**, were assessed for primary ADME properties. In general, solubility was high, Caco-2 permeability promising whereas mouse microsomal stability was low (Table 3).

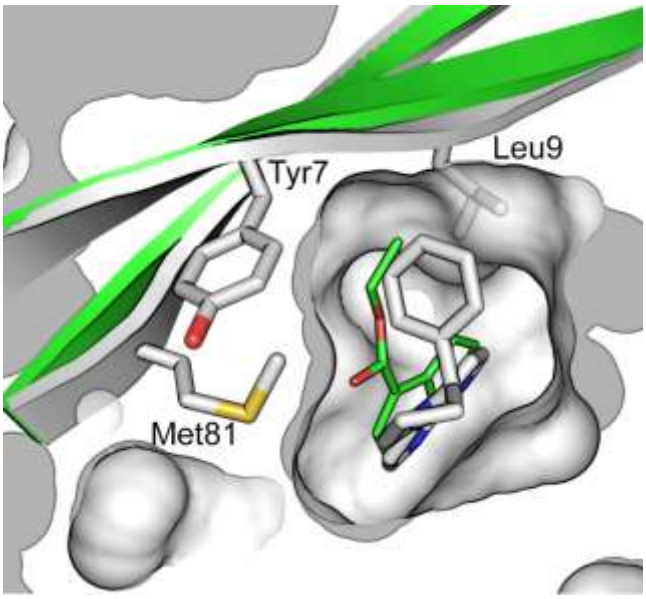

Figure 4. Overlay between the structure of MTH1-**16** (white) and MTH1-**1** (green). Compound **16** and compound **1** are displayed as thick and thin sticks respectively, with their carbon atoms colored following the same code as the secondary structure elements. The sidechains of MTH1 residues forming the cavity surrounding the phenyl moiety of **16** are displayed as sticks. Clipped molecular surface of MTH1 is shown in the MTH1-**16** complex structure (PDB ID: 6F23)

To determine whether a parallel SAR with respect to potency could be established, a few pyrrolidine-based substituents in the 4-position were combined with a small number of secondary amide substituents in the 2-position. Indeed, all combinations generated compounds (**20-25**) that were highly potent, some of them even below the assay wall of 0.1 nM (Table 3). When assessing Caco-2 permeability and metabolic stability, the most lipophilic representative (**20**) was clearly the most permeable but also the least metabolically stable analogue. Comparing to the more hydrophilic examples (**21-24**), it seemed reasonable to believe that microsomal stability was favored by decreasing lipophilicity, which in turn seemed unfavorable for permeability. This type of imbalance is commonly seen for small molecule drugs.[36] Still, we considered the compounds **24** and **25** as the most promising representatives in this series so far,

being highly potent, fairly stable in microsomes and with a medium Caco-2 permeability (Table 3).

Considering the very high potency of our compounds, we decided to deliberately discard the affinity-increasing amide-substituent in the 2-position, aiming to investigate whether the permeability and/or microsomal stability could be improved at the expense of potency. In the design process, we were also bearing in mind that increasing the fraction sp3-carbons and decreasing molecular weight and the number of aromatic rings may be favorable to improve drug properties.[31,36] We hypothesized that exchanging the carbon in the 2-position of the 7-azaindole core for a nitrogen would lead to a small decrease in lipophilicity, which might be beneficial for increasing metabolic stability.[37] More importantly, this extra nitrogen would remove the C-C double bond of this core, which we hypothesized could be significant for improving metabolic stability.[38] Thus, a set of the most promising 4-position substituents of earlier compounds and some additional new variations, were transferred to the 7-azaindazole core, creating compounds **26-30** (Table 3). Three of these showed biochemical potencies in the low nanomolar range, which is equivalent to the original 7-azaindole compounds, but as expected, neither of them were more potent than the corresponding 7-azaindole amide analogues. Permeability was very high for all of these small compounds (MW < 350), with no signs of efflux (Table 3). However, the metabolic stability was still low, and in fact all 7-azaindazole compounds were less stable than the 7-azaindole amide analogues. Also, the matched paired compounds **16** and **27**, with the 2-phenylpyrollidine substituent combined with the 7-azaindole and 7-azaindazole cores respectively, were equipotent and showed similar permeability, stability and solubility profiles.

The crystal structure of **29** showed a structural water within hydrogen-bonding distance from the newly introduced 2-position nitrogen of the 7-azaindazole core. Interestingly, this water is also at

hydrogen-bonding distance from both interaction points (Gly34 nitrogen and Asp120) of the earlier compounds with an amide substituent in the 2-position (Figure 5). While making hydrogen-bonding interactions with a structural water in some cases may increase potency[39,40], in our case, all matched-pair compounds (**9** and **26**, **20** and **27, 22** and **28**) clearly showed that the amide interactions were more important for potency than the corresponding interactions made by the structural water.

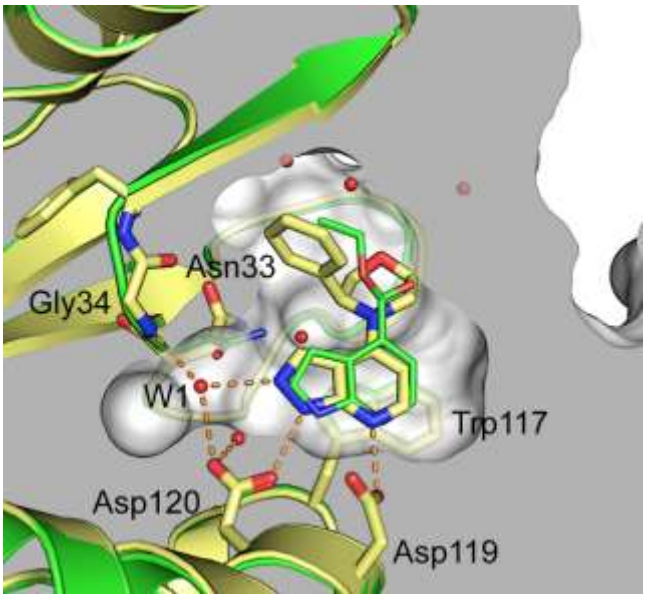

Figure 5. Overlay between the complex structure of MTH1-**29** (yellow) and MTH1-**1** (green). Compound **29** and **1** are displayed as thick and thin sticks, respectively with their carbon atoms colored following the same code as the secondary structure elements. Sidechain of MTH1 residues interacting with the compounds are shown as thin (**1**) and thick (**29**) sticks, respectively. Water molecules present in the binding site of **29** are depicted as red spheres. Hydrogen bond between MTH1, water molecules and **29** are displayed as orange dashes. Clipped molecular surface of MTH1 is shown in the MTH1-**29** complex structure (PDB ID: 6F22).

To assure a maintained high selectivity profile for the most promising representatives of our chemical series, compound **24** was tested in the same 97-membered kinase panel as compound **10**. Again**,** excellent selectivity was achieved [S-score = 0, Supporting information]. In addition, **24** was also tested in a 215-membered ATP-ase panel, including the structurally related MTH1-analogues NUDT2, NUDT3 and NUDT7. In summary, **24** was more than 1000 times selective against all additional anti-targets at 1 μM [Supporting information].

Cellular on-target engagement was another important property we wanted to verify for our MTH1-inhibitors. The most promising amide-containing compounds **20**, **24** and **25** were selected for evaluation, together with two less potent compounds **16** and **28**. These compounds were selected both as representatives for the different sub-series and to cover a biochemical potency range between 50 and 0.1 nM. TH588 was also included for comparisons.[8] To produce a reliable tool compound, we were aiming at creating compounds with a target engagement EC_{50} value that was more potent than the reference compound TH588. The compounds were evaluated in K562 cells in dose-response, using the cellular thermal shift assay (CETSA®).[41] There was a strong correlation between biochemical potency and CETSA EC_{50}. The three most potent compounds (**20**, **24** and **25**) had significantly higher CETSA EC_{50} values than the reference, and compounds **20** and **24** were 100 times more potent in both the biochemical and CETSA assays (Figure 6). Similar EC_{50} values of TH588 have been reported previously.[8,17]

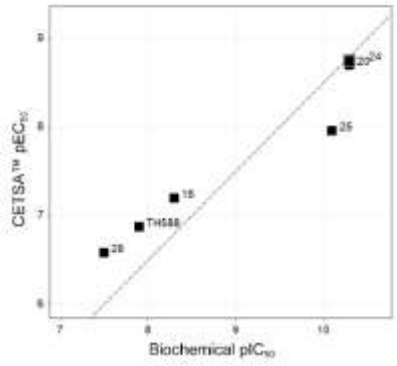

ID	CETSA™ pEC_{50}
TH588	6.9
28	6.6
16	7.2
20	8.7
24	8.7
25	8.0

Figure 6. There was a strong correlation between biochemical potency and target engagement in cells, using CETSA. Dotted line is showing y=x-1.5, indicating a drop-off from the biochemical assay to the cellular assay of about 30 times. Three compounds (**20**, **24** and **25**) had significantly higher pEC_{50} in CETSA than the reference TH588.

During the design process, a computational model was iteratively developed for predicting the potency of compounds in the 7-azaindole and 7-azaindazole series. The docking protocols usually predicted the correct binding mode, as assessed by crystal structures. Initially, substituents in the 4-position were prioritized for synthesis based only upon predicted binding mode of the final compound, primarily selecting the ones that allowed the core to maintain the same interaction mode to MTH1 as compound **1**. However, the docking score could not predict potency.[42] Considering the importance of the hydrogen-bond between the pyridine-type nitrogen N7 of the 7-azaindole ring and the Asp119 carboxylate, we combined the docking score and predicted pKa of N7 into a small partial-least-squares (PLS) model. This model was later fine-tuned by including a simple heavy atom count descriptor. During the optimization work, this model was continuously improved and used for selecting substituents in the 4-position., and the last iteration resulted in a predictive PLS model (R2 0.87), covering a potency range of more

than five log-units [Figure S3 and Table S2, Supporting information]. In a recent study, another docking-based model was used to virtually optimize fragments for MTH1-binding.[43]

Inspired by the importance of the pKa of N7 in the core structure, the high potency of the 7-azaindazole core, and considering that a large portion of a ligand's affinity to a protein usually comes from electronic interactions with key residues, the core itself was also subjected to further investigation.[44,45] Two matched pair variations of the azaindole and azaindazole cores, introducing an extra nitrogen in 3- and 5-position respectively, were synthesized. They were designed to investigate how these electronic variations would affect the hydrogen-bonding strength to the aspartates. None of them resulted in an improved potency (Table S3, Supporting information). To examine whether other nitrogen variations would be more favorable for affinity, another type of predictive potency model was developed. We were inspired by a previously published model, using density functional theory (DFT) calculations, where other types of core structures are interacting with two key aspartates of a protease.[46] Our model used the same methodology, and was used to predict the potency of three additional, virtual variations of the azaindole. However, since all three virtual compounds were suggested to be less potent than the original azaindole and azaindazole cores, we decided not to synthesize any additional variations (Figure S4, Supporting information).

To summarize the optimization-work so far, we decided to keep both the original 7-azaindole core and the secondary amide in the 2-position, since compounds such as **24** were combining the highest potencies in both the biochemical and CETSA assays with high kinome and ATPase selectivity, as well as showing the most promising permeability and stability profiles. In the next optimization cycle, we were aiming to fine-tune the ADME properties, with respect to Caco-2 permeability and metabolic stability. Using a combination of the collected SAR knowledge from

all previous compounds, the PLS potency model and the above mentioned medicinal chemistry rules of thumb, four new compounds (**31**-**34**) were designed with both new and previously used substituents in the 4-position. In these compounds, a combination of picomolar potency, high solubility, high permeability and acceptable metabolic stability was finally realized (Table 3).

Table 3 Biochemical potency, physicochemical properties, metabolic stability and Caco-2 permeability data for variations in 2- and 4-position substituents on the azaindole and azaindazole cores.

	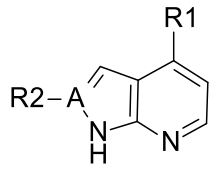			**Potency**		**Mouse liver microsomes**		**Caco-2 permeability**			**Physicochemical properties**		
ID	R1	A	R2	Biochemical IC_{50} (μM)	LE	mClint (μL/min/mg)	% Metabolised after 30 min	Papp A to B (10^{-6} cm/s)	Papp B to A (10^{-6} cm/s)	Efflux ratio	clogP	MW	Solubility in buffer (mM)
10		C		10	0.49	115	83	18	18	1	2.5	311.8	0.1
15		C	H	0.04	0.53	high	100	39	35	0.9	2.3	251.3	0.25
16	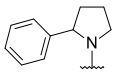	C	H	0.005	0.57	244	97	69	46	0.7	3.7	263.3	0.25
17	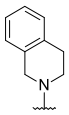	C	H	0.2	0.48						3.3	249.3	0.01
18	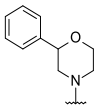	C	H	0.7	0.4						3.0	279.3	0.25
19		C	H	0.3	0.5						2.1	236.3	0.25
20	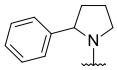	C		<0.0001	0.56	130	85	41	63	1.6	2.7	334.4	0.1
21	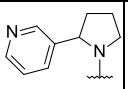	C		<0.0001	0.55	49	52	4	31	8.3	1.4	335.4	0.5

22	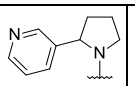	C	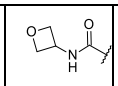	0.0001	0.5	24	29	1	1	0.7	0.8	363.4	0.25
23	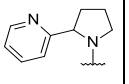	C		<0.0001	0.56	48	53	15	72	4.7	1.7	335.4	0.5
24	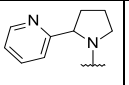	C		<0.0001	0.54	44	50	13	76	5.7	1.7	347.4	0.25
25	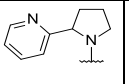	C	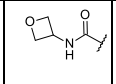	<0.0001	0.51	25	33	7	46	6.7	1.1	363.4	0.25
26	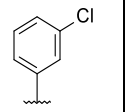	N		3	0.47						2.8	229.7	0.1
27	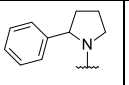	N		0.001	0.63	222	99	74	63	0.8	3.0	264.3	0.25
28	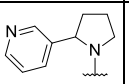	N		0.03	0.51	45	54	44	50	1.1	1.7	265.3	1
29	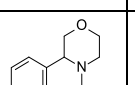	N		0.002	0.56	232	97	88	73	0.8	2.4	280.3	1
30	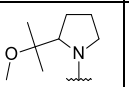	N		0.005	0.59	153	92	75	66	0.9	1.6	260.3	1
31 *	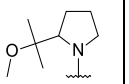	C		<0.0001	0.59	54	56	170	225	1,3	1.3	330.4	1
32 *	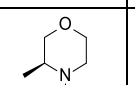	C		0.0008	0.59	36	43	148	209	1,4	0.6	288.3	0.5
33 *	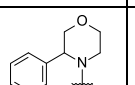	C		<0.0001	0.54	156	90	63	89	1,4	2.0	350.4	0.25
34 *	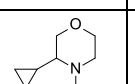	C		0.0001	0.59	45	48	24	79	3,3	1.0	314.4	0.5

*CaCo2-permeability measurements for compounds **31** - **34** were performed by an in-house method, as described in the experimental section. For all the other compounds the cell permeability was provided by Jubilant Life Sciences Ltd, as described in the experimental section.

Considering the promising properties of the four last compounds (**31**-**34**), they were nominated for additional *in vitro* studies, aiming at selecting one compound for *in vivo* efficacy studies. Complementary *in vitro* stability profiles were determined, using both human liver microsomes and rat hepatocytes. The overall highest stabilities were shown for compounds **32** and **34** (Table 4), also being the most stable in mouse microsomes (Table 3). The permeability profiles were also reevaluated internally, being aware of the commonly seen lab-to-lab variability in Caco-2 assays.[47] Given the higher A-B permeability and lower efflux ratio of **32** as compared to **34** (Table 3), we chose **32** as our probe compound, to be used in further *in vivo* studies. The *in vivo* bioavailability of **32** in mice was later shown to be high, and this probe molecule was extensively used to evaluate the potential of MTH1 inhibitors for the treatment of cancer.[1]

Table 4. *In vitro* stability for the four most optimized compounds.

	Human liver microsomes		**Rat hepatocytes**	
Compound	CL blood (L/h/kg)	Fmax (%)	CL blood (L/h/kg)	Fmax (%)
31	0,3	76,4	2,8	32,3
32*	0,3	78,4	0,5	87,3
33	0,6	57,4	3,5	17,8
34	0,4	72,4	1,4	67,6

* Compound 32 = BAY-707

In order to create a structurally related companion negative control probe, **32** was N-methylated in the 2-position, to disrupt the capability to interact with the key Asp120. Indeed, this methylated compound (**35**) demonstrated no activity in the MTH1 enzymatic assay until the highest concentration tested (20 μM). Furthermore, the physicochemical and pharmacokinetic

properties of **32** (named as BAY-707) and **35** (named as BAY-604) were evaluated, demonstrating similar or better profiles as compared to the reference compound TH588 (Figure 7 and Table S4, Supporting information). Finally, the selectivity profiles across 20 members of the NudiX family were assessed for both probe compounds, using TSA. A significant temperature shift (21 °C) was observed only for **32**, against its primary target MTH1, demonstrating the high selectivity of this new chemical matter (Figure S5 and Supporting information).

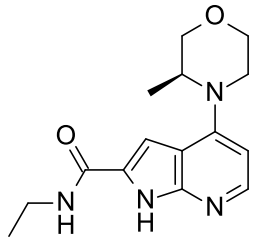

32
BAY-707
MTH1 positive probe

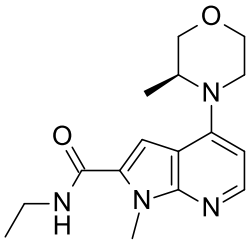

35
BAY-604
MTH1 negative probe

Figure 7. Compounds **32** and **35** were created as positive and negative probes for MTH1.

Conclusions

Starting from a generic, 10 μM fragment hit, a series of highly potent and selective MTH1 inhibitors were designed in a rational manner. Using fragment-based drug discovery methods and structure-based design, only 20 compounds were needed to improve biochemical potency by 10.000 times, while maintaining drug-like properties throughout the process, such as high ligand efficiency, high solubility and low lipophilicity. An additional 15 compounds were designed to improve the ADME properties, thus generating both permeable and stable compounds. As a result, the probe compound BAY-707 was created, allowing for extensive target validation work both *in vitro* and *in vivo*, when evaluating the potential of MTH1 inhibitors as a novel treatment of cancer.[1] Both BAY-707 and its companion negative control BAY-604 are now available as probe molecules at the Structural Genomics Consortium (SGC).

EXPERIMENTAL SECTION

Production of MTH1 enzyme. Full length human MTH1 was expressed and purified as previously described.[1]

Thermal shift assay. Purified MTH1 was screened against a library of 723 structurally diverse, soluble fragments. The thermal shift assay was performed in 96-well PCR plates (Bio-Rad) using a CFX96 Real-Time PCR Detection System (Bio-Rad). Protein unfolding was monitored using the fluorescent dye SYPRO Orange, which was purchased from Life Technologies as a 5000-times concentrated solution in 100% dimethyl sulfoxide (DMSO).

Each well contained 24 µL of 0.1 mg/mL of MTH1 protein in TSA buffer (20mM HEPES pH 7.5, 0.3M NaCl, 10% glycerol, 0.5mM TCEP) and 5x Sypro Orange dye. Fragments were added from a 25 mM master stock in 100% DMSO at a volume of 1 µL, yielding a final concentration of 1 mM in 4% (v/v) DMSO. 16 wells with MTH1 protein in 4% DMSO were used as reference samples in each plate. The plates were sealed with optically clear adhesive seals (Bio-Rad) and centrifuged at 1000 x *g* for 2 mins.

The fluorescence intensity data was acquired with excitation and emission wavelengths of 470 and 570 nm, respectively. The fluorescence was measured from 40 °C to 80 °C at a rate of 0.5 °C per 10 seconds. All measurements were carried out in duplicate and average values are reported.

The minimum and maximum fluorescence signal before and after the transition is used to determine the melting temperature, T_m, which is the inflection point of the sigmoidal denaturation curve. The raw data was exported to Microsoft Excel, and the T_m calculations were

performed in XLfit using a Boltzmann Sigmoidal fit. The ΔT_m for each fragment is calculated as the difference between the T_m in the presence and absence of fragments, $\Delta T_m = T_m(\text{fragment}) - T_m(\text{DMSO only})$. Significant thermal stabilization should be at least three times above the standard deviation of the DMSO controls, the initial hit cutoff value was set to +1.0 °C.

49 of the 166 initial hits were selected for retesting. Dilution series of the fragments were prepared in DMSO at 25 times the final assay concentration. MTH1 protein diluted in TSA buffer was added to the fragments as described above, giving final fragment concentrations from 62.5 to 1000 µM in 4% (v/v) DMSO ($n_1=n_0/2$ in 5 titration steps).

Isothermal titration calorimetry (ITC). An ITC200 microcalorimeter (MicroCal/GE Healthcare) was used to obtain the thermodynamic information of binding between MTH1 and fragment **1**. All the measurements were performed in a buffer composed of 20 mM Tris pH 7.5, 150 mM NaCl, 2 mM $MgCl_2$, 10 % glycerol, 0.5 mM TCEP. The calorimeter cell (volume 200 µL) was loaded with MTH1 protein at a concentration of 326 µM and the syringe was loaded with fragment **1** (dissolved in the same buffer) at a concentration of 3 mM in 1.5% DMSO (v/v). The DMSO concentrations in the cell and the syringe were carefully matched. Titrations were carried out at 25 °C with a stirring speed of 1000 rpm and each reaction had an initial delay of 60 s. Spacing between injections was kept at 150 s and the reference power at 8 µcal/s. The injection protocol included a single 0.4 µL first injection followed by 38 x 2 µL injections of the compound into the calorimeter cell.

Data were analyzed using Origin 7 software package and fitted well to a one-site binding model.

Crystallization of complex between compounds and MTH1. Protein sample was thawed, diluted to 1.8 mg/ml in 20 mM Tris-HCl pH 7.5, 150 mM sodium chloride, 5% glycerol, 2 mM TCEP and 6 mM magnesium chloride. For each complexes preparation, the protein solution was then supplemented respectively with either 0.25 mM (**7** and **16**) or 1 mM (**1** and **29**) of compound. Incubation occurred overnight at 4 °C. Complexes were then concentrated 10 times in an Amicon® Ultra (MWCO 10 kDa) (Millipore). Sample was centrifuged 30 min at 20000 × *g* (4 °C) and supernatant was used to set-up crystallization trials.

In a 96-well plate (vapor diffusion using sitting-drop), 0.15 µL of complex was mixed with 0.15 µL of a reservoir solution composed with either 23-27% PEG 6000, 0.2-0.3 M lithium sulfate and 0.1 M sodium acetate pH 3.6 (complexes with **7**, **16** and **1**) or 22% PEG 4000, 0.24 M ammonium sulfate and 12.5% glycerol (complex with **29**). Equilibration occurs against 50 µL of reservoir solution at either 18 °C (complexes with **7**, **16** and **1**) or 4 °C (complex with **29**). Rod-like crystals appeared within 6 days. Crystals were briefly soaked into a cryoprotecting-solution containing crystallization condition supplemented with 25% glycerol and then flash-frozen into liquid nitrogen.

Data collection, structure determination and refinement. Diffraction data were collected at the ESRF on the beamlines indicated in Table S1. Integration and scaling of data were performed using XDS.[48] Merging and truncating data were performed using the CCP4 suite of program.[49] Structures were solved by molecular replacement in Phaser[50] using BAY707-MTH1 structure (PDB code: 5NHY) as a model.[1] The asymmetric unit was composed with 2 molecules and compounds were manually placed in the difference Fourier electron density maps. Final models were produced using iterative cycles of manual model-building in Coot [51] and maximum-likelihood refinement in Refmac.[52] Furthermore, for MTH1-**16** complex, TLS refinement

(translation-libration-screw-rotation) were used during the latest stages of refinement using two TLS groups per monomer as identified by TLSMD[53] For MTH1-**29**, last stage of refinement was performed using anisotropic refinement in Refmac. The respective accession codes together with data processing and refinement statistics are reported in Table S1.

PPiLight biochemical assay. Dilution series of the compounds were prepared in DMSO at 100 times the final assay concentration ($n_1=n_0/3$ in 10 points). The compounds were further diluted to 5 times the assay concentration in assay buffer (40 mM Tris-HCl pH 7.5, 40 mM sodium chloride, 10 mM magnesium chloride, 1 mM DTT, 0.005% Tween 20). 2 µL of the diluted compounds were added to a 384 well assay plate followed by 2 µL of 0.5 nM enzyme (in-house produced full length human MTH1). Enzyme and compounds were pre-incubated at room temperature for 15 minutes. Then 6 µl of a substrate-converting-detection mixture (1 µL of 132 µM substrate (8-Oxo-2'-dGTP, TriLink Biotechnologies N-2034), 2.5 µL of converting reagent and 2.5 µL of detection reagent (PPiLight pyrophosphate Detection Kit, Lonza LT07-610)) was added to the wells containing compound and enzyme and mixing was performed by pipetting several times. The assay plate was incubated at room temperature for 1 hour and then read in a Victor 3V 1420 multilabel counter (Perkin Elmer), measurement time 0.1 seconds. Percent inhibition of the compounds as compared to dimethyl sulfoxide treated control samples was calculated. Compound concentration versus percent inhibition were fitted to generate IC_{50} values. Final compound concentration intervals are ranging from approximately 100x below to 100x above respective IC_{50} value. The final concentration enzyme is 0.1 nM which defines the limit for the IC_{50} values that can be measured in the assay.

Computational Chemistry. All computational chemistry work was done using Maestro 2016-3 from Schrödinger. Prior to docking studies and grid generation, the protein crystal structures were curated by preprocessing them in the Protein Preparation Wizard, using default settings. As the second step, hydrogen-bond assignment was done using default settings, and lastly a restrained minimization was performed, on hydrogens only. Crystallographic waters were removed in the active site, except for those structures that were used to dock the 7-azaindazoles (making a hydrogen-bond to the crystallographic water binding to Asp120).

Docking grids and sitemaps were created using default settings, defining the active site automatically around the crystallized ligand, belonging to each crystallized protein respectively. Asp 119 was protonated on the oxygen at closest distance to Trp123, to allow for a hydrogen-bond to the pyridine nitrogen of the core.

Glide dockings were done using default settings, without constraints.

The induced fit protocol was used for retrospectively predicting the correct binding mode of compound **5** using the crystal structure of compound **1.** Default settings were used, except for the box size which was reduced to save time: ”Dock ligands with length =<12Å”.

The PLS-based potency prediction model was created within the Partial Least-Squares Regression module in Canvas. Docking scores were generated as above, extracting the lowest glide score from each grid based on the crystal structures of **7**, **16** or **29**, the last one keeping the crystallographic water binding to Asp120. Heavy atom count (HAC) was calculated within Canvas. Predicted pKa values of the 7-azaindole acceptor-nitrogen were calculated with the Jaguar pKa-module, using default settings and water as solvent. Loading factors for the PLS-model were -0.27 for glide score, 0.85 for HAC and 0.45 for predicted pKa. Predicted potencies,

predicted pKa, glide scores and which compounds were used as training and test set are found in Table S2, Supporting information.

The DFT-based potency model was based on calculating the difference in energy (dE) between the protein-ligand complex in vacuum minus the energy of the protein alone in vacuum and the ligand alone, in water. The predicted energy difference (a negative value) was linearly fitted to the biochemical pIC_{50} values for the four synthesized compounds, using the equation $pred(pIC_{50}) = 3.1-0.31*dE$ (Table S3, Supporting information). Parts of the surrounding residues trp117, trp123 and phe72 were needed to keep the ligand in the correct position above the key residues Asp119 and Asp120 during energy optimization. Examples of the Jaguar input-files of how the energies were calculated for the ligand only, protein-ligand complex and the apo-structure are found the in the Supporting information. Basis set was lacvp+ and DFT method B3LYP. The starting position of the ligands were created via super-positioning of the core onto the crystal structure of **7**.

CETSA. Isothermal concentration response curves[41] were used to determine cellular target engagement potency of the compounds on MTH1.

K562 cells were cultured at 37 °C, 5% carbon dioxide in RPMI-1640 medium supplemented with 10% fetal bovine serum, 100 units/mL penicillin and 100 units/mL streptomycin. The cells were fed with half the volume additional fresh media a day prior to measurements. Cells of passage 16-19 that reached a density of 1.0-1.4 million/mL were used in the experiments. Intact K562 cells were pelleted by centrifugation and washed and re-suspended in HBSS at a cell density of 40 million cells/mL. The cell suspension was divided into 30 µL aliquots and an equal

volume of HBSS containing 2X the intended compound concentration was added, resulting in a final cell concentration of 20 million cells/mL. Up to 11 step dilution concentrations of the ligands in 1% DMSO were applied together with 1% DMSO only as control. The cells were incubated with ligand at 37 °C for 60 minutes, with gentle mixing every 10 minutes.

The aliquots were heated to a single specific temperature, 54 °C, as determined from established MTH1 melt and shift curves, for 3 minutes, and lysed by 3 cycles of freeze-thawing. Precipitated protein and cell debris were pelleted by centrifugation at 20000 × *g* for 20 minutes. Protein amounts were detected using standard Western Blot techniques. For detection of specific MTH1 bands the primary antibody sc-271082 (Santa Cruz Biotechnology) and the secondary antibody sc-2055 (Santa Cruz Biotechnology) together with Clarity Western ECL substrate (Bio-Rad) were used.

The Western Blot intensities were obtained by measuring the chemiluminescence counts per square mm and they were plotted normalized to a relevant control count. The isothermal concentration response data was analyzed and plotted using GraphPad Prism analysis and software. The obtained CETSA EC_{50} concentration response values represent the half maximal concentration the ligands for stabilizing MTH1 at 54 °C.

Caco-2 permeability assay. Caco-2 cells (purchased from ATCC) were seeded in DMEM 20% FBS at a density of 6 x 10^4 cells/well in a 24-well plate (Millicell Cell Culture) and cultured for 21 days with media replacement every 3 days. Monolayer integrity was assessed by measuring the transepithelial electrical resistance (TEER), and only wells with TEER values greater than

500 Ω cm^2 were considered for the permeability experiment. Digoxin was used as a control compound for efflux.

Test compound working stock solution at 10 µM were prepared by spiking 10 µL of the compound solution (10 mM in DMSO) in 9.990 mL transport media (TM)(HBSS buffer 10 mM HEPES, pH 7.4).

Experiments were performed in the apical (A) to basolateral (B) (A to B) as well as in the basolateral to apical (B to A). Cells were washed twice with TM and the cell filter plate was transferred to a 24-well transporter analysis plate containing either 1.0 mL TM per well (for A to B setup) or 10µM test compound and 5 µM reference compound (for B to A setup), in the receiver chamber. Permeability study was initiated by adding 0.3 mL of TM 10 µM of test compound or 5 µM of reference compound to donor chamber (A to B setup) or TM alone (B to A setup) in duplicates. Plates were incubated at 100 rpm and 37 °C and an aliquot of 100 µL was collected from donor as well as receiver chamber at intervals of time 0 and 60 minutes as indicated. After addition of equal volumes of acetonitrile containing IS (phenacetin, 200 ng/ml), samples centrifuged, and the cleared supernatants analyzed by LC-MS/MS.[54]

Caco-2 cell permeability assay for compounds 31-34. Caco-2 cells (purchased from DSMZ Braunschweig, Germany) were seeded at a density of 4.5 x 10^4 cell per well on 24 well insert plates, 0.4 µm pore size, and grown for 15 days in DMEM medium supplemented with 10% fetal bovine serum, 1% GlutaMAX (100x, GIBCO), 100 U/mL penicillin, 100µg/mL streptomycin (GIBCO) and 1% non-essential amino acids (100x) and cultured according to the providers specifications. Before running the permeation assay, the culture medium was replaced by a FBS-

free HEPES-carbonate transport puffer (pH 7.2). Monolayer integrity was assessed by measuring the transepithelial electrical resistance (TEER). Test compounds were added either to the apical or basolateral compartment to achieve 2 µM final concentration. Before and after 2 h incubation at 37 ºC, samples were taken from both compartments. Analysis of compound content was done after precipitation with methanol by LC/MS/MS analysis. The apparent permeability (P_{app}) was calculated using the following equation:

$$P_{app} = (V_r/P_o)(1/S)(P_2/t)$$

Where V_r is the volume of medium in the receiver chamber, P_o is the measured peak area of the test drug in the donor chamber at t=o, S the surface area of the monolayer, P_2 is the measured peak area of the test drug in the acceptor chamber after 2h of incubation, and t is the incubation time. The efflux ratio basolateral (B) to apical (A) was calculated by dividing the Papp B-A by the Papp A-B.

Metabolic stability assay in mouse liver microsomes. Assays were performed as previously described[55,56] with some modifications. Test compound or verapamil hydrochloride (reference compound) were added to 1 mL microsome suspension (Life Technologies [Gibco®], Inchinnan, UK) (550µg/ml in potassium phosphate buffer 66.7 mM, pH 7.4, PPB) to achieve a final concentration of 1 mM and 0.1% DMSO. Aliquots of 180 µL of the incubation mixture were taken at indicated times and incubated at 37 °C for 5 minutes. Then 20 µL of NAPDH solution (10 mM in PPB) were added to each tube, except for control samples which received 20 µL PPB. At the end of the incubation period 200 µL of quenching solution (0.05% formic acid in acetonitrile with 200 ng/mL phenacetin as internal standard) was added to stop the reaction. The

samples were centrifuged at 4000 rpm for 10 min and the supernatant was analysed by LC-MS/MS.

Calculation of microsomal intrinsic clearance (mCLint) was based on the test compound disappearance rate. The chromatographic peaks were integrated and the resultant peak area ratios between test compound or reference compound and IS were used for the calculations. A linear plot of the natural logarithm (ln) or the area ratio vs time was created to visualize the data and the slope was calculated for each data set. Subsequently, half-life (T1/2) and mCLint were calculated according to the following equations:

% Metabolized T_x= [1-(test area ratio Tx/test area ratio T_0)]*100, where x is 5, 15 and 30 minutes, respectively, area ratio is analyte peak area/IS peak area

Half Life (t1/2) (min) = ln2/-slope

mCLint (µL/min/mg) = (ln2 * 1000) / (t1/2 * [Microsomal protein]), where [Microsomal protein] is 0.5 mg/1000 µL.

Metabolic stability in rat hepatocytes. Hepatocytes from Han Wistar rats were isolated via a 2-step perfusion method. After perfusion, the liver was carefully removed from the rat: the liver capsule was opened, and the hepatocytes were gently shaken out into a Petri dish with ice-cold Williams' medium E (WME). The resulting cell suspension was filtered through sterile gaze in 50 mL falcon tubes and centrifuged at 50 × *g* for 3 min at room temperature. The cell pellet was resuspended in 30 mL WME and centrifuged through a Percoll® gradient for 2 times at 100 × *g*.

The hepatocytes were washed again with WME and resuspended in medium containing 5% FCS. Cell viability was determined by trypan blue exclusion.

For the metabolic stability assay liver cells were distributed in WME containing 5% FCS to glass vials at a density of 1.0×10^6 vital cells/mL. The test compound was added to a final concentration of 1 µM. During incubation, the hepatocyte suspensions were continuously shaken at 580 rpm and aliquots were taken at 2, 8, 16, 30, 45 and 90 min, to which equal volumes of cold methanol were immediately added. Samples were frozen at -20 °C overnight, after subsequently centrifuged for 15 minutes at 3000 rpm and the supernatant was analyzed with an Agilent 1200 HPLC-system with LCMS/MS detection.

The half-life of a test compound was determined from the concentration-time plot. From the half-life the intrinsic clearances were calculated using the `well stirred´ liver model together with the additional parameters liver blood flow, amount of liver cells *in vivo* and *in vitro*. The hepatic *in vivo* blood clearance (CL) and the maximal oral bioavailability (Fmax) was calculated. The following parameter values were used: Liver blood flow = 4.2 L/h/kg rat; specific liver weight – 32 g/kg rat body weight; liver cells *in vivo* - 1.1×10^8 cells/g liver, liver cells *in vitro* – 1.0×10^6 cells/mL.

Metabolic stability in human liver microsomes. The *in vitro* metabolic stability of test compounds was determined by incubating them at 1 µM in a suspension liver microsomes in 100 mM phosphate buffer, pH 7.4 ($NaH_2PO_4 \times H_2O + Na_2HPO_4 \times 2H_2O$) and at a protein concentration of 0.5 mg/mL at 37 °C. The microsomes were activated by adding a co-factor mix containing 8 mM Glucose-6-Phosphate, 4 mM $MgCl_2$; 0.5 mM NADP and 1 IU/mL G-6-P-Dehydrogenase in phosphate buffer, pH 7.4. The metabolic assay was started shortly afterwards

by adding the test compound to the incubation at a final volume of 1 mL. Organic solvent in the incubations was limited to ≤0.01 % dimethylsulfoxide (DMSO) and ≤1% acetonitrile. During incubation, the microsomal suspensions were continuously shaken at 580 rpm and aliquots were taken at 2, 8, 16, 30, 45 and 60 min, to which equal volumes of cold methanol were immediately added. Samples were frozen at -20 °C overnight, subsequently centrifuged for 15 minutes at 3000 rpm and the supernatant was analyzed with an Agilent 1200 HPLC-system with LCMS/MS detection.

The half-life of a test compound was determined from the concentration-time plot. From the half-life the intrinsic clearances were calculated. Together with the additional parameters liver blood flow, specific liver weight and microsomal protein content the hepatic *in vivo* blood clearance (CL) and the maximal oral bioavailability (Fmax) were calculated using the `well stirred´ liver model. The following parameter values were used: Liver blood flow – 1.32 L/h/kg; specific liver weight – 21 g/kg; microsomal protein content – 40 mg/g.

Chemistry. Unless otherwise stated, all solvents, reagents and starting materials used were commercially available and were used without further purification. Reactions requiring anhydrous conditions were run in dried equipment using anhydrous solvents under an inert atmosphere of nitrogen or argon. Room temperature refers to 20-25 °C. Microwave heating was performed in a Biotage® Initiator Microwave Synthesiser at the indicated temperature in the recommended microwave tubes.

^{1}H NMR spectra were recorded in the indicated deuterated solvent at 400 MHz or 500 MHz and the spectra were obtained unless stated otherwise, using a Bruker AV400 NMR or Bruker 500MHz Avance NMR spectrometer with a probe of suitable configuration. Chemical shifts are reported in ppm from lowest to highest. Resonance multiplicities are denoted s, d, t, q, m and br for singlet, doublet, triplet, quartet, multiplet, and broad respectively.

Preparative HPLC was performed on a Gilson HPLC system with a UV detector using an XBridge® Prep C18 5 µm 30x75 mm column with acetonitrile / 0.2% NH_3 in MilliQ gradient or a YMC-Pack® ODS-AQ C18 5 µm 30x150 mm column with acetonitrile / 0.2% acetic acid in MilliQ gradient. Flow rate: 35 mL/min. Flash chromatography was performed using a Combi Flash® Companion™ system using Silicycle™ normal-phase flash columns.

Purity and mass analyses were performed on an LC-MS consisting of an Agilent 1100 system with a G1322A Degasser, G1312A Binary Pump, G1313A Autosampler, G1316A Column Oven, G1365B Multi Wavelength Detector and G1946D Mass Spectrometer. The mass spectrometer was equipped with an electrospray ion source (ES) operated in positive ion mode. For separation a linear gradient was applied starting at 90 % 0.1% NH_3 in MilliQ ending at 90% acetonitrile on a XTerra® RP18 3.5 µm 3.0x50mm column at a flow rate of 1 ml/min for 3 min or a linear gradient starting at 90% 0.1% acetic acid in MilliQ ending at 90% acetonitrile on a

Symmetry® C18 3.5 µm 3.0x50mm column at a flow rate of 1 ml/min for 3 min. Purity of final compounds was assessed by reversed-phase HPLC with UV detection at 214 nm. All tested compounds demonstrated HPLC purity ≥95%.

4-(1*H*-Pyrrolo[2,3-b]pyridin-5-yl)-1*H*-pyrrolo[2,3-*b*]pyridine (2)

5-Bromo-1*H*-pyrrolo[2,3-*b*]pyridine (100 mg, 0.51 mmol), tert-butyl 4-(4,4,5,5-tetramethyl-1,3,2-dioxaborolan-2-yl)pyrrolo[2,3-b]pyridine-1-carboxylate (192 mg, 0.56 mmol), potassium carbonate (140 mg, 1.0 mmol) and [1,1′-bis(diphenylphosphino)ferrocene]dichloropalladium(II) (4.1 mg, 0,0051 mmol) were dissolved in 1,2-dimethoxyethane (5 mL). The mixture was heated to 100 °C in a sealed tube. The suspension was filtered and purified by preparative RP-HPLC, ammonia buffer to give 10 mg (8%) of the title compound. ^{1}H NMR (500 MHz, Methanol-d_4) δ ppm 6.65 (d, J = 3.47 Hz, 1 H), 6.74 (d, J = 3.47 Hz, 1 H), 7.30 (d, J = 5.04 Hz, 1 H), 7.51 (dd, J = 6.62, 3.47 Hz, 2 H), 8.29 (d, J = 4.73 Hz, 1 H), 8.42 (d, J = 1.89 Hz, 1 H), 8.61 - 8.64 (m, 1 H). MS (ES+) *m/z* 235 $[M+H]^+$.

4-(3-Pyridyl)-1*H*-pyrrolo[2,3-*b*]pyridine (3)

4-Chloro-1*H*-pyrrolo[2,3-*b*]pyridine (250 mg, 1.6 mmol) and 1*H*-pyrazole (279 mg, 4.1 mmol) were taken up in 1,4-dioxane (1.5 mL). Then, saturated aqueous ammonium formate (1.5 mL) and iodine (1.04 g, 4.1 mmol) were added and the resulting mixture was stirred at room temperature for 16 h. A saturated aqueous solution of sodium thiosulfate (3 mL) and ethyl acetate (10 mL) were added. The phases were separated, and the aqueous phase was extracted with ethyl acetate (2 x 10 mL). The combined organic phases were washed with brine, dried over sodium sulfate, filtered and concentrated to give a yellow solid. The material was then

recrystallized from methanol to give 240 mg (67%) of 4-chloro-2-pyrazol-1-yl-1*H*-pyrrolo[2,3-*b*]pyridine as a white solid. ^{1}H NMR (400MHz, DMSO-d_6) δ ppm 6.64 (s, 1 H), 6.69 (s, 1 H), 7.24 (d, *J* = 5.0 Hz, 1 H), 7.87 (s, 1 H), 8.15 (d, *J* = 5.3 Hz, 1 H), 8.57 (s, 1 H), 12.97 (br. s., 1 H). MS (ES+) *m/z* 219 $[M+H]^+$. A portion of this material (140 mg, 0.64 mmol), bis(di-tert-butyl(4-dimethylaminophenyl)phosphine)dichloropalladium(II) (23 mg, 0.032 mmol), potassium carbonate (265 g, 1.9 mmol) and 3-pyridylboronic acid (94 mg, 0.77 mmol) were taken up in a mixture of 1,4-dioxane:H_2O:EtOH (6:3:1) (2 mL) and the resulting mixture was heated in a microwave reactor at 150 °C for 75 min. The mixture was filtered and purified by preparative RP-HPLC, ammonia buffer to give 18 mg (14%) of the title compound as a beige solid. ^{1}H NMR (400MHz, DMSO-d_6) δ ppm 6.63 (br. s., 1 H), 7.26 (d, *J* = 4.8 Hz, 1 H), 7.64 - 7.52 (m, 2 H), 8.18 (d, *J* = 8.1 Hz, 1 H), 8.32 (d, *J* = 4.8 Hz, 1 H), 8.67 (d, *J* = 4.5 Hz, 1 H), 8.97 (s, 1 H), 11.89 (br. s., 1 H). MS (ES+) *m/z* 196 $[M+H]^+$.

4-(3-Chlorophenyl)-1*H*-pyrrolo[2,3-*b*]pyridine (4)

4-Chloro-1*H*-pyrrolo[2,3-*b*]pyridine (100 mg, 0.66 mmol), (3-chlorophenyl)boronic acid (102 mg, 0.66 mmol), bis(di-tert-butyl(4-dimethylaminophenyl)phosphine)dichloropalladium(II) (46 mg, 0.066 mmol) and potassium carbonate (181 mg, 1.3 mmol) were taken up into acetonitrile (6 mL) and water (1 mL). The mixture was heated in a microwave reactor at 120 °C for 30 min. The organic layer was collected, filtered and was purified by preparative RP-HPLC, ammonia buffer to give 20 mg (13%) of the title compound. ^{1}H NMR (500 MHz, DMSO-d_6) δ ppm 6.54 - 6.68 (m, 1 H), 7.23 (d, *J* = 5.04 Hz, 1 H), 7.49 - 7.68 (m, 3 H), 7.69 - 7.86 (m, 2 H), 8.31 (d, *J* = 5.04 Hz, 1 H), 11.88 (br s, 1 H). MS (ES+) *m/z* 229 $[M+H]^+$.

_N_-Methyl-4-(3-pyridyl)-1_H_-pyrrolo[2,3-_b_]pyridine-2-carboxamide (5)

n-Butyllitium (4.1 mL, 1.6 M in hexanes, 6.6 mmol), was added slowly to a solution of diisopropylamine (1 mL, 7.1 mmol) in 2-methyltetrahydrofuran (20 mL) at 0 °C. The reaction was stirred at 0 °C for 5 min and then cooled to -78 °C. A solution of 1-(benzenesulfonyl)-4-chloro-pyrrolo[2,3-*b*]pyridine (1.63 g, 5.6 mmol) in 2-methyltetrahydrofuran (10 mL) was added dropwise. The resulting mixture was stirred at -78 °C for 15 min and then allowed to heat to room temperature. After stirring for another 10 min, the mixture was again cooled to -78 °C. Ethyl chloroformate (0.7 mL, 7.3 mmol) was added dropwise and the resulting mixture was stirred on the thawing cooling bath for 30 min and then at room temperature for 30 min. Saturated aqueous ammonium chloride was added followed by water and ethyl acetate. The organic layer was separated, and the aqueous layer was extracted twice with ethyl acetate. The combined organic phases were washed with aqueous hydrochloric acid (1 M) and brine, dried over sodium sulfate and concentrated. The crude product was dissolved in dichloromethane, passed through a plug of silica gel and concentrated to give 2.0 g of ethyl 1-(benzenesulfonyl)-4-chloro-pyrrolo[2,3-*b*]pyridine-2-carboxylate (MS (ES+) *m/z* = 365 $[M+H]^+$). A portion of this material (150 mg, 0.41 mmol), bis(di-tert-butyl(4-dimethylaminophenyl)phosphine)dichloropalladium(II) (15 mg, 0.02 mmol), 3-pyridylboronic acid (66 mg, 0.53 mmol) and potassium carbonate (170 mg, 1.2 mmol) were taken up in a mixture of 1,4-dioxane:H_2O:EtOH (6:3:1) (2 mL) and the resulting mixture was heated in a microwave reactor at 150 °C for 15 min. Methylamine (1 mL, 40% in water, 12 mmol) was added and the mixture was heated in a microwave reactor at 150 °C for 15 min. The reaction mixture was filtered and purified by preparative RP-HPLC, ammonia buffer to give 12 mg (12%) of the title compound over several steps from ethyl 1-(benzenesulfonyl)-4-chloro-pyrrolo[2,3-

b]pyridine-2-carboxylate. ^{1}H NMR (400 MHz, DMSO-d_6) δ ppm 2.82 (br d, J = 3.78 Hz, 3 H), 7.32 (br d, J = 4.53 Hz, 1 H), 7.35 (s, 1 H), 7.59 - 7.65 (m, 1 H), 8.20 (br d, J = 7.81 Hz, 1 H), 8.42 (d, J = 4.78 Hz, 1 H), 8.54 - 8.66 (m, 1 H), 8.71 (br d, J = 5.04 Hz, 1 H), 9.01 (s, 1 H). MS (ES+) m/z 253 $[M+H]^+$.

4-(3-Chlorophenyl)-*N*-methyl-1*H*-pyrrolo[2,3-*b*]pyridine-2-carboxamide (6)

Ethyl 1-(benzenesulfonyl)-4-chloro-pyrrolo[2,3-*b*]pyridine-2-carboxylate (2.4 g, 6.6 mmol), (3-chlorophenyl)boronic acid (1.13 g, 7.2 mmol), potassium carbonate (2.27 g, 16 mmol) and bis(di-tert-butyl(4-dimethylaminophenyl)phosphine)dichloropalladium(II) (0.23 g, 0.33 mmol) were dissolved in acetonitrile (10 mL) and water (5 mL). The reaction was heated in a microwave reactor at 120 °C for 2 h. The mixture was diluted with ethyl acetate and water. The phases were separated, and the organic phase was concentrated. The formed residue was recrystallized from 2-propanol to give 2.0 g of ethyl 1-(benzenesulfonyl)-4-(3-chlorophenyl)pyrrolo[2,3-*b*]pyridine-2-carboxylate (MS (ES+) *m/z* 441 $[M+H]^+$) which was dissolved in methanol (20 mL), tetrahydrofuran (10 mL) and water (5 mL). Lithium hydroxide monohydrate (0.95 g, 23 mmol) was added and the resulting mixture was stirred at 50 °C for 16 h. The mixture was concentrated, and the resulting residue was dissolved in water. Concentrated hydrochloric acid was added to acidify the solution, which was then kept in refrigerator for 30 min. The resulting precipitate was collected by suction filtration, washed with water and dried to give 700 mg of 4-(3-chlorophenyl)-1*H*-pyrrolo[2,3-*b*]pyridine-2-carboxylic acid as an orange solid. A portion of this material (50 mg, 0.18 mmol), methylamine (0.18 mL, 2 M in ethanol, 0.37 mmol), *O*-(benzotriazol-1-yl)-*N,N,N′,N′*-tetramethyluronium hexafluorophosphate (83 mg,

0.22 mmol) and triethylamine (0.051 mL, 0.37 mmol) were dissolved in *N,N*-dimethylformamide (1 mL). The reaction was stirred at room temperature for 16 h. The reaction mixture was diluted with methanol, filtered and purified by preparative RP-HPLC, ammonia buffer to give 7 mg (5%) of the title compound over several steps from ethyl 1-(benzenesulfonyl)-4-chloro-pyrrolo[2,3-*b*]pyridine-2-carboxylate. ^{1}H NMR (500MHz, DMSO-d_6) δ ppm 2.83 (d, J = 4.41 Hz, 3 H), 7.27 - 7.30 (m, 1 H), 7.30 - 7.34 (m, 1 H), 7.57 - 7.67 (m, 2 H), 7.74 - 7.78 (m, 1 H), 7.80 - 7.84 (m, 1 H), 8.35 - 8.48 (m, 1 H), 8.56 - 8.66 (m, 1 H), 12.34 (br s, 1 H). MS ES+ 286 *m/z* $[M+H]^+$

4-(3-Chlorophenyl)-*N*-ethyl-1*H*-pyrrolo[2,3-*b*]pyridine-2-carboxamide (7)

4-(3-Chlorophenyl)-1*H*-pyrrolo[2,3-b]pyridine-2-carboxylic acid (120 mg, 0.44 mmol), ethylamine (0.44 mL, 2 M in tetrahydrofuran, 0.88 mmol), *O*-(benzotriazol-1-yl)-*N,N,N′,N′*-tetramethyluronium hexafluorophosphate (200 mg, 0.53 mmol) and triethylamine (0.12 mL, 0.88 mmol) were dissolved in *N,N*-dimethylformamide (2 mL). The reaction was stirred at room temperature for 16 h. The reaction mixture was filtered and purified by preparative RP-HPLC, ammonia buffer to give 9 mg (2%) of the title compound over several steps from ethyl 1-(benzenesulfonyl)-4-chloro-pyrrolo[2,3-*b*]pyridine-2-carboxylate. ^{1}H NMR (500 MHz, Chloroform-*d*) δ ppm 1.33 (t, J = 7.25 Hz, 3 H), 3.60 (quin, J = 6.78 Hz, 2 H), 6.36 (br s, 1 H), 6.98 (s, 1 H), 7.23 (d, J = 4.73 Hz, 1 H), 7.45 - 7.54 (m, 2 H), 7.63 (br d, J = 6.94 Hz, 1 H), 7.74 (s, 1 H), 8.65 (d, J = 4.73 Hz, 1 H), 11.25 (br s, 1 H). MS ES+ 300 *m/z* $[M+H]^+$

4-(3-Chlorophenyl)-*N,N*-dimethyl-1*H*-pyrrolo[2,3-*b*]pyridine-2-carboxamide (8)

4-(3-Chlorophenyl)-1*H*-pyrrolo[2,3-*b*]pyridine-2-carboxylic acid (200 mg, 0.73 mmol), dimethylamine (0.73 mL, 2 M in tetrahydrofuran, 1.5 mmol), *O*-(benzotriazol-1-yl)-*N,N,N′,N′*-tetramethyluronium hexafluorophosphate (330 mg, 0.88 mmol) and triethylamine (0.2 mL, 1.5 mmol) were dissolved in *N,N*-dimethylformamide (1 mL). The reaction was stirred at room temperature for 16 h. The reaction mixture was diluted with methanol, filtered and purified by preparative RP-HPLC, ammonia buffer to give 7 mg (1%) of the title compound over several steps from ethyl 1-(benzenesulfonyl)-4-chloro-pyrrolo[2,3-*b*]pyridine-2-carboxylate. ^{1}H NMR (400 MHz, DMSO-d_6) δ ppm 3.06 (br s, 3 H), 3.21 (br s, 3 H), 6.88 (d, *J* = 2.01 Hz, 1 H), 7.28 (d, *J* = 4.78 Hz, 1 H), 7.55 - 7.63 (m, 2 H), 7.72 - 7.79 (m, 1 H), 7.80 (s, 1 H), 8.40 (d, *J* = 4.78 Hz, 1 H), 12.32 (br s, 1 H). MS ES+ *m/z* 300 $[M+H]^+$.

4-(3-Chlorophenyl)-1*H*-pyrrolo[2,3-*b*]pyridine-2-carboxamide (9)

4-(3-Chlorophenyl)-1*H*-pyrrolo[2,3-*b*]pyridine-2-carboxylic acid (300 mg, 1.1 mmol) and oxalyl dichloride (0.11 mL, 1.3 mmol) were dissolved in dichloromethane (5 mL). One drop of *N,N*-dimethylformamide was added and the mixture was stirred at room temperature for 1 h. The mixture was concentrated under reduced pressure and the residue was dissolved in dichloromethane. Ammonia was bubbled though the mixture for 30 min. The mixture was concentrated, and the crude solid was crystallized from 2-propanol to give 10 mg (1%) of the title compound over several steps from ethyl 1-(benzenesulfonyl)-4-chloro-pyrrolo[2,3-*b*]pyridine-2-carboxylate. ^{1}H NMR (500MHz, DMSO-d_6) δ ppm 7.29 (d, *J* = 4.73 Hz, 1 H), 7.34 - 7.40 (m, 1 H), 7.50 (br s, 1 H), 7.61 (s, 2 H), 7.77 (br d, *J* = 7.75 Hz, 1 H), 7.82 (s, 1 H), 8.00 - 8.15 (m, 1 H), 8.42 (d, *J* = 4.73 Hz, 1 H), 12.21 - 12.34 (m, 1 H). MS ES+ 272 *m/z* $[M+H]^+$

4-(3-Chlorophenyl)-*N*-cyclopropyl-1*H*-pyrrolo[2,3-*b*]pyridine-2-carboxamide (10)

4-(3-Chlorophenyl)-1*H*-pyrrolo[2,3-*b*]pyridine-2-carboxylic acid (50 mg, 0.18 mmol), cyclopropylamine (25 µL, 0.367 mmol), *O*-(benzotriazol-1-yl)-*N,N,N′,N′*-tetramethyluronium hexafluorophosphate (83 mg, 0.22 mmol) and triethylamine (0.051 mL, 0.37 mmol) were dissolved in *N,N*-dimethylformamide (1 mL). The reaction was stirred at room temperature for 16 h. The reaction mixture was diluted with methanol, filtered and purified by preparative HPLC to give 16 mg (11%) of the title compound over several steps from ethyl 1-(benzenesulfonyl)-4-chloro-pyrrolo[2,3-*b*]pyridine-2-carboxylate. ^{1}H NMR (500 MHz, DMSO-d_6) δ ppm 0.56 - 0.63 (m, 2 H), 0.69 - 0.79 (m, 2 H), 2.87 (br d, *J* = 4.41 Hz, 1 H), 7.28 (d, *J* = 4.73 Hz, 1 H), 7.31 (s, 1 H), 7.57 - 7.66 (m, 2 H), 7.75 (d, *J* = 7.57 Hz, 1 H), 7.80 (s, 1 H), 8.41 (d, *J* = 4.73 Hz, 1 H), 8.58 (br d, *J* = 4.10 Hz, 1 H), 12.30 (br s, 1 H). MS ES+ 312 *m/z* $[M+H]^+$

4-(3-Chlorophenyl)-2-methyl-1*H*-pyrrolo[2,3-*b*]pyridine (11)

1-(Benzenesulfonyl)-4-chloro-2-methyl-pyrrolo[2,3-*b*]pyridine (740 mg, 2.4 mmol), bis(pinacolato)diboron (796 mg, 3.1 mmol) and potassium acetate (710 mg, 7.2 mmol) were taken up in 1,4-dioxane (10 mL) and the reaction was put under nitrogen atmosphere. 2-Dicyclohexylphosphino-2′,6′-dimethoxybiphenyl (59 mg, 0.14 mmol) and palladium(II) acetate (16 mg, 0.07 mmol) were added and the resulting mixture was stirred at 100 °C for 16 h. LCMS showed ~50% conversion to product and some de-chlorinated starting material. More bis(pinacolato)diboron (400 mg, 1.5 mmol), 2-dicyclohexylphosphino-2′,6′-dimethoxybiphenyl (59 mg, 0.14 mmol) and palladium(II) acetate (16 mg, 0.07 mmol) were added and the resulting

mixture was stirred at 100 °C for 5 h. When cooled to room temperature the mixture was filtered, concentrated and purified on a silica gel column eluted with 0-50% ethyl acetate in n-heptane to give 890 mg of 1-(benzenesulfonyl)-2-methyl-4-(4,4,5,5-tetramethyl-1,3,2-dioxaborolan-2-yl)pyrrolo[2,3-*b*]pyridine (MS (ES+) 399 *m/z* $[M+H]^+$). A portion of this material (150 mg, 0.38 mmol), 1-bromo-3-chloro-benzene (72 mg, 0.38 mmol), potassium carbonate (156 g, 1.13 mmol) and bis(di-tert-butyl(4-dimethylaminophenyl)phosphine)dichloropalladium(II) (13 mg, 0.02 mmol) were dissolved in acetonitrile (2 mL) and water (1 mL). The mixture was heated in a microwave reactor at 120 °C for 40 min. After cooling lithium hydroxide monohydrate (95 mg, 23 mmol) was added and the mixture was heated in a microwave reactor at 100 °C for 1 h. The phases were separated, and the organic phase was filtered and purified by preparative HPLC to give 3 mg (3%) of the title compound over several steps from 1-(benzenesulfonyl)-4-chloro-2-methyl-pyrrolo[2,3-*b*]pyridine. ^{1}H NMR (500 MHz, Methanol-d_4) δ ppm 2.49 (s, 3 H), 6.34 (s, 1 H), 7.14 (d, J = 5.04 Hz, 1 H), 7.43 - 7.48 (m, 1 H), 7.49 - 7.54 (m, 1 H), 7.68 (d, J = 7.57 Hz, 1 H), 7.73 (s, 1 H), 8.14 (d, J = 5.04 Hz, 1 H). MS (ES+) 243 *m/z* $[M+H]^+$

4-(3-Chlorophenyl)-1*H*-pyrrolo[2,3-*b*]pyridine-2-carbonitrile (12)

4-(3-Chlorophenyl)-1*H*-pyrrolo[2,3-*b*]pyridine-2-carboxylic acid (500 mg, 1.8 mmol) was taken up in thionyl chloride (3 mL, 41 mmol) and the resulting mixture was stirred at 80 °C for 15 min. The mixture was concentrated, and the resulting residue was dissolved in tetrahydrofuran (5 mL) and then slowly added to aqueous ammonia (10 mL, 25%) at 0 °C. The cooling bath was removed, and the resulting mixture was stirred at room temperature for 30 min. The mixture was concentrated under reduced pressure to remove ammonia and tetrahydrofuran to give a yellow aqueous suspension. Ethyl acetate (5 mL) was added and the mixture was stirred at room

temperature for 10 min. The resulting precipitate was collected by suction filtration, washed with ethyl acetate, pentane and dried to give 300 mg of **9** as a yellow solid. This material was taken up in phosphorous oxychloride (1 mL, 11 mmol) and the resulting mixture was stirred at 100 °C for 1.5 h. When cooled to room temperature ice was added followed by saturated aqueous sodium bicarbonate and aqueous ammonia (25%). The formed precipitate was collected by suction filtration, washed with water and dried. The solid was suspended in dichloromethane (5 mL) and the precipitate was collected by suction filtration, washed with dichloromethane and dried. The solid was purified by preparative RP-HPLC, ammonia buffer to give 10 mg (1%) the title compound as a solid. ^{1}H NMR (400MHz, DMSO-d_6) δ ppm 8.53 (d, J = 4.5 Hz, 1 H), 7.82 - 7.78 (m, 1 H), 7.78 - 7.73 (m, 1 H), 7.62 - 7.55 (m, 2 H), 7.51 (s, 1 H), 7.36 (d, J = 4.5 Hz, 1 H). MS ES+ *m/z* 254 $[M+H]^+$.

5-[4-(3-Chlorophenyl)-1*H*-pyrrolo[2,3-*b*]pyridin-2-yl]oxazole (13)

n-Butyllithium (2.8 mL, 2.5 M in hexanes, 7.0 mmol) was added slowly to a solution of diisopropylamine (1 mL, 7.1 mmol) in 2-methyltetrahydrofuran (15 mL) at 0 °C. The resulting mixture was stirred at 0 °C for 5 min and was then cooled to -78 °C. A solution of 1-(benzenesulfonyl)-4-chloro-pyrrolo[2,3-*b*]pyridine (1.5 g, 5.1 mmol) in 2-methyltetrahydrofuran (10 mL) was added dropwise. The resulting mixture was stirred at -78 °C for 20 min and then the mixture was allowed to reach room temperature. The mixture was stirred at room temperature for 10 min to give a suspension and then cooled to -78 °C again. *N,N*-Dimethylformamide (1.2 mL, 16 mmol) was added dropwise and the resulting mixture was stirred on the thawing cooling bath for 30 min and then at room temperature for 30 min. Saturated aqueous ammonium chloride (12 mL) was added and the phases were separated. The aqueous phase was extracted with ethyl

acetate (2 x 10 mL) and the combined organic phases were washed with hydrochloric acid (20 mL, 0.5 M) followed by brine (15 mL). The solution was dried over sodium sulfate, filtered and concentrated to give the intermediate 1-(benzenesulfonyl)-4-chloro-pyrrolo[2,3-*b*]pyridine-2-carbaldehyde as an orange gum, which was used without any further purification. This material, (3-chlorophenyl)boronic acid (205 mg, 1.3 mmol), bis(triphenylphosphine)dichloropalladium(II) (38 mg, 0.06 mmol) and potassium carbonate (452 mg, 3.3 mmol) were taken up in 1,4-dioxane (5 mL) and water (1 mL) and the resulting mixture was stirred at 90 °C for 2 h. The reaction was cooled to room temperature and brine (5 mL) was added. The mixture was extracted with ethyl acetate (2 x 5 mL). The combined organic phases were concentrated and purified on a silica gel column eluted with 0-40% ethyl acetate in n-heptane to give 200 mg of the intermediate 1-(benzenesulfonyl)-4-(3-chlorophenyl)pyrrolo[2,3-b]pyridine-2-carbaldehyde as a yellow solid. This material, potassium carbonate (70 mg, 0.50 mmol) and *p*-toluenesulfonylmethyl isocyanide (98 mg, 0.50 mmol) were taken up in absolute ethanol (10 mL) and the resulting mixture was stirred at 70 °C for 15 min. Methanol (5 mL) was added to dissolve the starting material and the resulting mixture was stirred at 70 °C for 1 h. Lithium hydroxide monohydrate (63 mg, 1.5 mmol) and water (1 mL) were added and the mixture was stirred at 70 °C for 1.5 h. The reaction was cooled to room temperature and concentrated. The resulting residue was taken up in ethyl acetate (10 mL) and water (5 mL). The phases were separated, and the aqueous phase was extracted with ethyl acetate (2 x 10 mL). The combined organic phases were washed with saturated aqueous sodium bicarbonate followed by brine. The solution was dried over sodium sulfate, filtered and concentrated. The crude product was recrystallized from methanol to give 45 mg (3%) of the title compound over several steps from 1-(benzenesulfonyl)-4-chloro-pyrrolo[2,3-*b*]pyridine. ^{1}H NMR (400MHz, DMSO-d_6) δ ppm 6.94 (d, J = 2.0 Hz, 1 H), 7.28 (d,

J = 5.0 Hz, 1 H), 7.64 - 7.54 (m, 2 H), 7.73 (s, 1 H), 7.82 - 7.75 (m, 2 H), 8.35 (d, *J* = 4.8 Hz, 1 H), 8.53 (s, 1 H), 12.61 (s, 1 H). MS ES+ *m/z* 296 $[M+H]^+$.

[4-(3-Chlorophenyl)-1*H*-pyrrolo[2,3-*b*]pyridin-2-yl]methanol (14)

4-(3-Chlorophenyl)-1*H*-pyrrolo[2,3-*b*]pyridine-2-carboxylic acid (200 mg, 0.73 mmol) was dissolved in dichloromethane (15 mL). Lithium aluminium hydride (111 mg, 2.9 mmol) was added to the solution and the mixture was stirred for 1 h. The reaction was cooled to 0 °C and quenched with water (0.1 mL) followed by aqueous sodium hydroxide (15%) (0.1 mL) and water (0.3 mL). After stirring for 1 h at room temperature, the mixture was filtered and the solid was rinsed with ether. The combined organic phases were concentrated and purified by preparative RP-HPLC, ammonia buffer to give 12 mg (2%) of the title compound over several steps from ethyl 1-(benzenesulfonyl)-4-chloro-pyrrolo[2,3-*b*]pyridine-2-carboxylate. ^{1}H NMR (500 MHz, DMSO-d_6) δ ppm 4.64 (s, 2 H), 5.33 (br s, 1 H), 6.47 (s, 1 H), 7.18 (d, *J* = 5.04 Hz, 1 H), 7.51 - 7.56 (m, 1 H), 7.56 - 7.63 (m, 1 H), 7.73 (d, *J* = 7.57 Hz, 1 H), 7.76 (s, 1 H), 8.23 (d, *J* = 4.73 Hz, 1 H), 11.77 (br s, 1 H). MS ES+ *m/z* 259 $[M+H]^+$.

4-(1*H*-Pyrrolo[2,3-*b*]pyridin-4-yl)-2,3-dihydro-1,4-benzoxazine (15)

4-Chloro-1*H*-pyrrolo[2,3-*b*]pyridine (100 mg, 0.66 mmol), 3,4-dihydro-2*H*-1,4-benzoxazine (177 mg, 1.3 mmol), (2-dicyclohexylphosphino-2′,4′,6′-triisopropyl-1,1′-biphenyl)[2-(2-aminophenyl)phenyl)]palladium(II) chloride (25 mg, 0.033 mmol) and sodium *tert*-butoxide (126 mg, 1.3 mmol) were taken up in 1,4-dioxane (2 mL) and the resulting mixture was stirred at 100 °C for 16 h in a sealed tube. The reaction was cooled to room temperature and brine (2 mL) and ethyl acetate (3 mL) were added. The phases were separated, and the aqueous phase was

extracted with ethyl acetate (3 mL). The combined organic phases were concentrated and purified by preparative RP-HPLC, ammonia buffer to give 37 mg (23%) of the title compound as a white solid. ^{1}H NMR (500MHz, DMSO-d_6) δ ppm 3.97 - 3.88 (m, 2 H), 4.29 - 4.18 (m, 2 H), 6.20 (dd, J = 1.6, 3.2 Hz, 1 H), 6.78 - 6.73 (m, 1 H), 6.80 (d, J = 5.4 Hz, 1 H), 6.87 - 6.82 (m, 1 H), 6.94 - 6.88 (m, 2 H), 7.34 (t, J = 2.8 Hz, 1 H), 8.08 (d, J = 5.4 Hz, 1 H), 11.60 (br. s., 1 H). MS (ES+) *m/z* 252 $[M+H]^+$.

4-(2-phenylpyrrolidin-1-yl)-1*H*-pyrrolo[2,3-*b*]pyridine (16)

4-Chloro-1*H*-pyrrolo[2,3-*b*]pyridine (100 mg, 0.66 mmol) and 2-phenylpyrrolidine (289 mg, 2.0 mmol) were dissolved in *N*-methyl-2-pyrrolidone (1 mL) The mixture was heated in a microwave reactor at 210 °C for 1 h. After cooling the mixture was diluted with methanol, filtered and purified by preparative RP-HPLC, ammonia buffer to give 60 mg (33%) of the title compound. ^{1}H NMR (500 MHz, DMSO-d_6) δ ppm 1.80 - 1.88 (m, 1 H), 1.88 - 1.96 (m, 1 H), 1.96 - 2.04 (m, 1 H), 2.35 - 2.46 (m, 1 H), 3.76 - 3.86 (m, 1 H), 4.06 (br t, J = 7.25 Hz, 1 H), 5.19 (br d, J = 6.62 Hz, 1 H), 5.87 (d, J = 5.36 Hz, 1 H), 6.42 (br s, 1 H), 7.00 (br s, 1 H), 7.17 - 7.22 (m, 1 H), 7.22 - 7.27 (m, 2 H), 7.27 - 7.36 (m, 2 H), 7.67 (d, J = 5.67 Hz, 1 H), 11.13 (br s, 1 H). MS (ES+) *m/z* 264 $[M+H]^+$.

2-(1*H*-Pyrrolo[2,3-*b*]pyridin-4-yl)-3,4-dihydro-1*H*-isoquinoline (17)

4-Chloro-1*H*-pyrrolo[2,3-*b*]pyridine (100 mg, 0.66 mmol) and 1,2,3,4-tetrahydroisoquinoline (0.25 mL, 2.0 mmol) were taken up in *N*-methyl-2-pyrrolidone (1 mL) and heated in a microwave reactor at 200 °C for 1 h. The reaction was cooled to room temperature and diluted with methanol (1 mL). The mixture was left standing at room temperature for 1 h. The resulting

precipitate was collected by suction filtration, washed with methanol and dried to give the crude product as a white solid. Recrystallized from 2-propanol to give 27 mg (17%) of the title compound as a white solid. ^{1}H NMR (400MHz, DMSO-d_6) δ ppm 2.99 (t, J = 5.8 Hz, 2 H), 3.80 (t, J = 5.8 Hz, 2 H), 4.63 (s, 2 H), 6.45 (d, J = 5.5 Hz, 1 H), 6.58 (d, J = 3.5 Hz, 1 H), 7.24 - 7.16 (m, 4 H), 7.29 - 7.24 (m, 1 H), 7.93 (d, J = 5.5 Hz, 1 H), 11.37 (br. s., 1 H). MS (ES+) *m/z* 250 $[M+H]^+$.

2-Phenyl-4-(1*H*-pyrrolo[2,3-*b*]pyridin-4-yl)morpholine (18)

4-Chloro-1*H*-pyrrolo[2,3-*b*]pyridine (107 mg, 0.70 mmol), 2-phenylmorpholine (149 mg, 0.91 mmol) and *N,N*-diisopropylethylamine (0.18 mL, 1.0 mmol) were taken up in *N*-methyl-2-pyrrolidone (0.6 mL) and the resulting mixture was heated in a microwave reactor at 220 °C for 1 h. The reaction was cooled to room temperature and diluted with methanol (1 mL). The resulting mixture was filtered and purified by preparative RP-HPLC, ammonia buffer to give 97 mg (50%) of the title compound as a light-yellow solid. ^{1}H NMR (500 MHz, DMSO-d_6) δ ppm 2.80 - 2.89 (m, 1 H), 3.07 (td, J = 11.98, 3.15 Hz, 1 H), 3.83 - 3.97 (m, 3 H), 4.12 (dd, J = 11.35, 2.21 Hz, 1 H), 4.69 - 4.81 (m, 1 H), 6.47 (d, J = 5.36 Hz, 1 H), 6.51 (d, J = 2.84 Hz, 1 H), 7.26 (br. s., 1 H), 7.29 - 7.36 (m, 1 H), 7.38 (t, J = 7.41 Hz, 2 H), 7.48 (d, J = 7.25 Hz, 2 H), 7.96 (d, J = 5.67 Hz, 1 H), 11.45 (br. s., 1 H). MS (ES+) *m/z* 280 $[M+H]^+$.

4-(2,3-Dihydropyrrolo[2,3-*b*]pyridin-1-yl)-1*H*-pyrrolo[2,3-*b*]pyridine (19)

4-Chloro-1*H*-pyrrolo[2,3-*b*]pyridine (78 mg, 0.51 mmol), 2,3-dihydro-1*H*-pyrrolo[2,3-*b*]pyridine (74 mg, 0.61 mmol), (2-dicyclohexylphosphino-2′,4′,6′-triisopropyl-1,1′-biphenyl)[2-(2-aminophenyl)phenyl)]palladium(II) chloride (2.0 mg, 2.6 μmol) and lithium

bis(trimethylsilyl)amide (1.21 mL, 1.06 M in hexanes, 1.3 mmol) were dissolved in 2-methyltetrahydrofuran (5 mL), The mixture was heated in a microwave reactor at 100 °C for 1 h. After cooling the mixture was concentrated. The residue was dissolved in methanol, filtered and purified by preparative RP-HPLC, ammonia buffer to give 8 mg (7%) of the title compound. ^{1}H NMR (500 MHz, DMSO-d_6) δ ppm 3.21 (t, J = 8.35 Hz, 2 H), 4.48 (t, J = 8.35 Hz, 2 H), 6.65 (dd, J = 3.47, 1.58 Hz, 1 H), 6.80 (dd, J = 7.09, 5.20 Hz, 1 H), 7.28 - 7.33 (m, 1 H), 7.56 (dd, J = 7.25, 1.26 Hz, 1 H), 7.97 - 8.06 (m, 3 H), 11.50 (br s, 1 H). MS (ES+) *m/z* 237 $[M+H]^+$.

_N_-Ethyl-4-(2-phenylpyrrolidin-1-yl)-1_H_-pyrrolo[2,3-_b_]pyridine-2-carboxamide (20)

Ethyl 1-(benzenesulfonyl)-4-chloro-pyrrolo[2,3-*b*]pyridine-2-carboxylate (700 mg, 1.9 mmol) and 2-phenylpyrrolidine (706 mg, 4.8 mmol) were dissolved in *N*-methyl-2-pyrrolidone (2 mL) and the resulting mixture was heated in a microwave reactor at 160 °C for 1 h. After being cooled to room temperature, the mixture was diluted with ethyl acetate and water. The phases were separated, and the aqueous phase was extracted twice with ethyl acetate. The combined organic phases were concentrated and the crude product was recrystallized from ethyl acetate to give 350 mg (53%) of ethyl 4-(2-phenylpyrrolidin-1-yl)-1*H*-pyrrolo[2,3-*b*]pyridine-2-carboxylate. ^{1}H NMR (500 MHz, DMSO-d_6) δ ppm 1.29 (t, J = 7.09 Hz, 3 H), 1.82 - 1.90 (m, 1 H), 1.90 - 1.98 (m, 1 H), 1.98 - 2.07 (m, 1 H), 2.37 - 2.47 (m, 1 H), 3.86 (br. s., 1 H), 4.13 (br. s., 1 H), 4.26 (q, J = 6.94 Hz, 2 H), 5.19 (br. s., 1 H), 5.89 (br. s., 1 H), 7.17 - 7.27 (m, 4 H), 7.28 - 7.33 (m, 2 H), 7.81 (d, J = 5.36 Hz, 1 H), 12.02 (br. s., 1 H). MS (ES+) *m/z* 336 $[M+H]^+$. A portion of this material (215 mg, 0.64 mmol) was suspended in methanol (10 mL), tetrahydrofuran (5 mL) and water (2 mL) and lithium hydroxide monohydrate (108 mg, 2.6 mmol) was added. The reaction mixture was stirred at 50 °C for 16 h and then concentrated. The

resulting crude product was dissolved in water and concentrated hydrochloric acid was added to acidify the solution. The formed precipitate was isolated by suction filtration and dried to give 190 mg (96%) of 4-(2-phenylpyrrolidin-1-yl)-1*H*-pyrrolo[2,3-*b*]pyridine-2-carboxylic acid. ^{1}H NMR (500 MHz, DMSO-d_6) δ ppm 1.76 - 2.12 (m, 3 H), 2.35 - 2.47 (m, 1 H), 3.85 (br. s., 1 H), 4.11 (br. s., 1 H), 5.21 (br. s., 1 H), 5.90 (br. s., 1 H), 7.13 (br. s., 1 H), 7.18 - 7.26 (m, 3 H), 7.28 - 7.34 (m, 2 H), 7.80 (d, *J* = 5.67 Hz, 1 H), 11.88 (br. s., 1 H), 12.69 (br. s., 1 H). MS (ES+) *m/z* 308 $[M+H]^+$. A portion of this material (120 mg, 0.39 mmol) was taken up in thionyl chloride (2 mL, 28 mmol) and the resulting mixture was stirred at 80 °C for 1 h. The reaction mixture was concentrated, and the resulting residue was taken up in tetrahydrofuran (10 mL) and cooled to 0 °C. Ethylamine (6 mL, 1M in tetrahydrofuran, 6.0 mmol) was added and the mixture was stirred at room temperature for 1 h. The formed precipitate was isolated by suction filtration and washed with tetrahydrofuran and recrystallized from 2-propanol. Purification by preparative RP-HPLC, ammonia buffer gave 48 mg (36%) of the title compound. ^{1}H NMR (500 MHz, DMSO-d_6) δ ppm 1.14 (t, *J* = 7.25 Hz, 3 H), 1.81 - 1.90 (m, 1 H), 1.93 - 2.10 (m, 2 H), 2.39 - 2.48 (m, 1 H), 3.25 - 3.31 (m, 2 H), 3.88 - 4.03 (m, 1 H), 4.13 - 4.28 (m, 1 H), 5.04 - 5.17 (m, 1 H), 5.79 (d, *J* = 5.67 Hz, 1 H), 7.17 - 7.27 (m, 3 H), 7.27 - 7.37 (m, 3 H), 7.71 (d, *J* = 5.67 Hz, 1 H), 8.19 - 8.26 (m, 1 H), 11.52 (br. s., 1 H). MS (ES+) *m/z* 335 $[M+H]^+$.

_N_-ethyl-4-[2-(3-pyridyl)pyrrolidin-1-yl]-1*H*-pyrrolo[2,3-*b*]pyridine-2-carboxamide (21)

Ethyl 1-(benzenesulfonyl)-4-chloro-pyrrolo[2,3-*b*]pyridine-2-carboxylate (1 g, 2.7 mmol) and 3-pyrrolidin-2-ylpyridine (1 g, 6.8 mmol) were dissolved in *N*-methyl-2-pyrrolidone (2 mL) and the resulting mixture was heated in a microwave reactor at 160 °C for 3 h. After being cooled to room temperature, the reaction mixture was diluted with water and ethyl acetate. The phases

were separated, and the aqueous phase was extracted twice with ethyl acetate. The combined organic phases were diluted with methanol and washed with brine, dried over sodium sulfate and concentrated. The residue was passed through a silica gel column (0-10% methanol in dichloromethane with 7 mM ammonia added) and evaporated. The resulting material was suspended in tetrahydrofuran (15 mL) and water (5 mL) and lithium hydroxide monohydrate (474 mg, 11 mmol), was added. The reaction mixture was stirred at 50 °C. After 90 min, methanol (10 mL) was added and the stirring was continued at 50 °C for 16 h. The solvents were evaporated, and the resulting crude product was dissolved in water. Concentrated hydrochloric acid was added to acidify the solution and the mixture was kept at 5 °C for 3 h. The formed precipitate was isolated by suction filtration, washed with water and dried to give 680 mg of 4-[2-(3-pyridyl)pyrrolidin-1-yl]-1*H*-pyrrolo[2,3-*b*]pyridine-2-carboxylic acid (MS (ES+) *m/z* 309 $[M+H]^+$). A portion of this material (120 mg, 0.39 mmol) was taken up in thionyl chloride (2 mL, 27 mmol) and the reaction was stirred at 80 °C for 2.5 h. The mixture was concentrated, and the resulting residue was dissolved in tetrahydrofuran (10 mL) and cooled to 0 °C. Ethylamine (6 mL, 1M in tetrahydrofuran, 6.0 mmol) was added and the mixture was stirred at room temperature for 15 min. Dimethyl sulfoxide (1 mL) was added and the resulting mixture was stirred at room temperature for 16 h. The formed precipitate was isolated by suction filtration, washed with tetrahydrofuran and dried. The crude product was recrystallized from 2-propanol to give 27 mg (16%) of the title compound over several steps from ethyl 1-(benzenesulfonyl)-4-chloro-pyrrolo[2,3-*b*]pyridine-2-carboxylate. ^{1}H-NMR (500 MHz, DMSO-d_6) δ ppm 1.14 (s, 3 H), 1.84 - 2.13 (m, 3 H), 2.42 - 2.49 (m, 1 H), 3.24 - 3.31 (m, 2 H), 3.86 - 4.03 (m, 1 H), 4.17 - 4.30 (m, 1 H), 5.11 - 5.28 (m, 1 H), 5.72 - 5.91 (m, 1 H), 7.28 - 7.38 (m, 2 H), 7.58 - 7. 66 (m, 1

H), 7.70 - 7.77 (m, 1 H), 8.19 - 8.28 (m, 1 H), 8.39 - 8.46 (m, 1 H), 8.49 - 8.57 (m, 1 H), 11.26 - 11.90 (m, 1 H). MS (ES+) m/z 336 $[M+H]^+$.

_N_-(Oxetan-3-yl)-4-[2-(3-pyridyl)pyrrolidin-1-yl]-1_H_-pyrrolo[2,3-_b_]pyridine-2-carboxamide (22)

4-[2-(3-Pyridyl)pyrrolidin-1-yl]-1*H*-pyrrolo[2,3-*b*]pyridine-2-carboxylic acid (120 mg, 0.39 mmol) was taken up in thionyl chloride (2 mL, 27 mmol) and the resulting mixture was stirred at 80 °C for 3 h. The mixture was concentrated and the resulting residue was taken up in tetrahydrofuran (10 mL) and cooled to 0 °C. A solution of oxetan-3-amine (0.14 mL, 2.0 mmol) and *N*,*N*-diisopropylethylamine (0.34 mL, 2.0 mmol) in tetrahydrofuran (2 mL) was added and the mixture was stirred at room temperature for 15 min. Dimethyl sulfoxide (1 mL) was added and the resulting mixture was stirred at room temperature for 16 h. The mixture was concentrated, and the resulting residue was diluted with ethyl acetate (10 mL) stirred at room temperature for 15 min and then kept at 5 °C for 1 h. The resulting precipitate was filtered off, washed with ethyl acetate and discarded. The filtrate was concentrated and purified by preparative RP-HPLC, ammonia buffer to give 48 mg (27%) of the title compound over several steps from ethyl 1-(benzenesulfonyl)-4-chloro-pyrrolo[2,3-*b*]pyridine-2-carboxylate. ^{1}H-NMR (500 MHz, DMSO-d_6) δ ppm 1.91 (br d, J = 2.5 Hz, 1 H), 1.99 – 2.16 (m, 2 H), 2.44 - 2.50 (m, 1 H), 3.97 (br d, 1 H), 4.26 (br s, 1 H), 4.58 (q, J = 6.0 Hz, 2 H), 4.82 (t, J = 6.8 Hz, 2 H), 4.96 – 5.11 (m, 1 H), 5.19 (br d, J = 5.7 Hz, 1 H), 5.80 (br d, J = 5.4 Hz, 1 H), 7.32 (dd, J = 4.9, 7.7 Hz, 1 H), 7.47 (br s, 1 H), 7.63 (d, J = 7.7 Hz, 1 H), 7.75 (d, J = 5.7 Hz, 1 H), 8.43 (dd, J = 1.6, 4.7 Hz, 1 H), 8.52 (d, J = 1.6 Hz, 1 H), 8.93 (br d, J = 6.9 Hz, 1 H), 11.67 (br s, 1 H). MS (ES+) *m/z* 364 $[M+H]^+$.

_N_-ethyl-4-[2-(2-pyridyl)pyrrolidin-1-yl]-1_H_-pyrrolo[2,3-_b_]pyridine-2-carboxamide (23)

Ethyl 1-(benzenesulfonyl)-4-chloro-pyrrolo[2,3-*b*]pyridine-2-carboxylate (1.0 g, 2.7 mmol), 2-pyrrolidin-2-ylpyridine (1.02 g, 6.8 mmol) and *N*,*N*-diisopropylethylamine (0.49 mL, 2.7 mmol) were dissolved in *N*-methyl-2-pyrrolidone (2 mL). The mixture was heated in a microwave reactor at 180 °C for 1 h. Water and ethyl acetate were added. The phases were separated and the organic phase was washed with water, dried over magnesium sulfate and evaporated to give 800 mg of ethyl 4-[2-(2-pyridyl)pyrrolidin-1-yl]-1*H*-pyrrolo[2,3-*b*]pyridine-2-carboxylate (MS (ES+) *m/z* 337 $[M+H]^+$). A portion of this material (460 mg, 1.4 mmol) was taken up in tetrahydrofuran (5 mL), methanol (10 mL) and water (5 mL) and lithium hydroxide monohydrate (230 mg, 5.5 mmol) was added. The resulting mixture was stirred at 50 °C for 2 h. The solvents were evaporated, and the resulting crude product was dissolved in water. Concentrated hydrochloric acid was added to acidify the solution and the mixture was kept at 5 °C for 3 h. The formed precipitate was isolated by suction filtration, washed with water and dried to give 360 mg of 4-[2-(2-pyridyl)pyrrolidin-1-yl]-1*H*-pyrrolo[2,3-*b*]pyridine-2-carboxylic acid (MS (ES+) *m/z* 309 $[M+H]^+$). A portion of this material (130 mg, 0.42 mmol) was taken up in thionyl chloride (2 mL, 27 mmol) and the resulting mixture was stirred at 80 °C for 2.5 h. The mixture was concentrated, and the resulting residue was taken up in tetrahydrofuran (10 mL) and cooled to 0 °C. Ethylamine (5 mL, 2M in tetrahydrofuran, 10 mmol) was added and the mixture was stirred at room temperature for 15 min. The reaction mixture was concentrated and purified by preparative RP-HPLC, ammonia buffer to give 46 mg (24%) of the title compound over several steps from ethyl 1-(benzenesulfonyl)-4-chloro-pyrrolo[2,3-*b*]pyridine-2-carboxylate. ^{1}H-NMR (500 MHz, DMSO-d_6) δ ppm 1.15 (t, J = 7.1 Hz, 3 H), 1.96 - 2.08 (m, 3 H), 2.41 - 2.49 (m, 1 H),

3.25 - 3.33 (m, 2 H), 3.96 (br d, 1 H), 4.21 (br s, 1 H), 5.06 - 5.20 (m, 1 H), 5.80 (br d, 1 H), 7.20 (d, 1 H), 7.25 (t, 1 H), 7.32 (br s, 1 H), 7.69 (t, 1 H), 7.75 (d, 1 H), 8.24 (br s, 1 H), 8.57 (d, 1 H), 11.63 (br s, 1 H). MS (ES+) *m/z* 336 $[M+H]^+$.

_N_-cyclopropyl-4-[2-(2-pyridyl)pyrrolidin-1-yl]-1_H_-pyrrolo[2,3-_b_]pyridine-2-carboxamide (24)

4-[2-(2-Pyridyl)pyrrolidin-1-yl]-1*H*-pyrrolo[2,3-*b*]pyridine-2-carboxylic acid (120 mg, 0.39 mmol) was taken up in thionyl chloride (2 mL, 27 mmol) and the resulting mixture was stirred at 80 °C for 1 h. The mixture was concentrated, and the resulting residue was taken up in tetrahydrofuran (10 mL) and cooled to 0 °C. Cyclopropylamine (156 mg, 2.7 mmol) was added and the mixture was stirred at room temperature for 15 min. Dimethyl sulfoxide (1 mL) was added and the mixture was stirred at room temperature for 16 h. The formed precipitate was isolated by suction filtration, washed with tetrahydrofuran and dried. The crude product was purified by preparative RP-HPLC, ammonia buffer to give 62 mg (33%) of the title compound over several steps from ethyl 1-(benzenesulfonyl)-4-chloro-pyrrolo[2,3-*b*]pyridine-2-carboxylate. ^{1}H NMR (500 MHz, DMSO-d_6) δ ppm 0.56 (br s, 2 H), 0.73 (br d, J = 5.04 Hz, 2 H), 1.96 - 2.11 (m, 3 H), 2.40 - 2.49 (m, 1 H), 2.82 (br d, J = 3.78 Hz, 1 H), 3.96 (br s, 1 H), 4.20 (br s, 1 H), 5.12 (br s, 1 H), 5.79 (br s, 1 H), 7.19 (d, J = 7.88 Hz, 1 H), 7.22 - 7.28 (m, 1 H), 7.30 (br s, 1 H), 7.69 (br t, J = 7.09 Hz, 1 H), 7.73 (br d, J = 5.67 Hz, 1 H), 8.24 (br s, 1 H), 8.56 (br d, J = 4.10 Hz, 1 H), 11.50 (br s, 1 H). MS (ES+) *m/z* 348 $[M+H]^+$.

_N_-(oxetan-3-yl)-4-[2-(2-pyridyl)pyrrolidin-1-yl]-1_H_-pyrrolo[2,3-_b_]pyridine-2-carboxamide (25)

4-[2-(2-Pyridyl)pyrrolidin-1-yl]-1*H*-pyrrolo[2,3-*b*]pyridine-2-carboxylic acid (50 mg, 0.16 mmol) was taken up in thionyl chloride (1 mL, 14 mmol), and the resulting mixture was stirred at 80 °C for 2 h. The mixture was concentrated, and the resulting residue was taken up in 1,4-dioxane (2 mL). A solution of oxetan-3-amine (70 µL, 1.0 mmol) and *N*,*N*-diisopropylethylamine (0.14 mL, 0.81 mmol) in 1,4-dioxane (1 mL) was added and the reaction mixture was stirred at room temperature for 1 h. The reaction mixture was concentrated and purified by preparative RP-HPLC, ammonia buffer to give 16 mg (20%) of the title compound over several steps from ethyl 1-(benzenesulfonyl)-4-chloro-pyrrolo[2,3-*b*]pyridine-2-carboxylate. ^{1}H NMR (500 MHz, DMSO-d_6) δ ppm 1.94 - 2.15 (m, 3 H), 2.39 - 2.49 (m, 1 H), 4.00 (br s, 1 H), 4.24 (br s, 1 H), 4.55 - 4.62 (m, 2 H), 4.82 (t, *J* = 6.78 Hz, 2 H), 4.99 - 5.08 (m, 1 H), 5.14 (br s, 1 H), 5.80 (br s, 1 H), 7.21 (d, *J* = 7.88 Hz, 1 H), 7.23 - 7.28 (m, 1 H), 7.44 (br s, 1 H), 7.69 (br t, *J* = 7.57 Hz, 1 H), 7.74 (br d, *J* = 5.36 Hz, 1 H), 8.57 (br d, *J* = 4.73 Hz, 1 H), 8.92 (br d, *J* = 6.94 Hz, 1 H), 11.61 (br s, 1 H). MS (ES+) *m/z* 364 $[M+H]^+$.

4-(3-Chlorophenyl)-1*H*-pyrazolo[3,4-*b*]pyridine (26)

4-Chloro-1*H*-pyrazolo[3,4-*b*]pyridine (100 mg, 0.65 mmol), (3-chlorophenyl)boronic acid (122 mg, 0.78 mmol), bis(triphenylphosphine)dichloropalladium(II) (23 mg, 0.033 mmol) and potassium carbonate (270 mg, 1.95 mmol) were taken up in a mixture of 1,4-dioxane:H_2O:EtOH (2 mL, 6:3:1) and the resulting mixture was heated in a microwave reactor at 150 °C for 30 min. The mixture was left standing at room temperature for 1 h and the resulting precipitate was collected by suction filtration, washed with water, 1,4-dioxane and pentane and finally dried to give 29 mg (19%) of the title compound as a white solid.

^{1}H NMR (400 MHz, DMSO-d_6) δ ppm 7.41 (d, J = 4.78 Hz, 1 H), 7.59 - 7.66 (m, 2 H), 7.78 - 7.88 (m, 1 H), 7.89 (s, 1 H), 8.32 (s, 1 H), 8.60 (d, J = 4.78 Hz, 1 H), 13.86 (br s, 1 H). MS (ES+) *m/z* 230 $[M+H]^+$.

4-(2-Phenylpyrrolidin-1-yl)-1*H*-pyrazolo[3,4-*b*]pyridine (27)

4-Chloro-1*H*-pyrazolo[3,4-*b*]pyridine (70 mg, 0.46 mmol) and 2-phenylpyrrolidine (134 mg, 0.91 mmol) were mixed with *N*-methyl-2-pyrrolidone (0.3 mL). The mixture was heated in a microwave reactor at 180 °C for 1h. The mixture was diluted with methanol (3 mL) and stirred for 10 min. The solid was collected by suction filtration and washed with 2-propanol and pentane and finally air dried to give 40 mg (33%) of the title compound. ^{1}H NMR (500 MHz, DMSO-d_6) δ ppm 1.89 (br d, J = 9.46 Hz, 1 H), 1.96 (br d, J = 7.25 Hz, 1 H), 2.03 (br s, 1 H), 2.40 - 2.48 (m, 1 H), 3.79 (br s, 1 H), 4.07 (br s, 1 H), 5.23 (br s, 1 H), 5.87 (br s, 1 H), 7.18 - 7.27 (m, 3 H), 7.31 (br t, J = 7.41 Hz, 2 H), 7.88 (br s, 2 H), 13.01 (br s, 1 H). MS (ES+) *m/z* 265 $[M+H]^+$.

4-[2-(3-Pyridyl)pyrrolidin-1-yl]-1*H*-pyrazolo[3,4-*b*]pyridine (28)

4-Chloro-1*H*-pyrazolo[3,4-*d*]pyrimidine (78 mg, 0.50 mmol) and 3-pyrrolidin-2-ylpyridine (110 mg, 0.76 mmol) were dissolved in *N*-methyl-2-pyrrolidone (1 mL). The mixture was heated in a microwave reactor at 220 °C for 30 min and then concentrated. The residue was dissolved in methanol, filtered and purified by preparative RP-HPLC, acetic acid buffer to give 20 mg (11%) of the title compound. ^{1}H NMR (500 MHz, DMSO-d_6) δ ppm 1.89 - 2.03 (m, 2 H), 2.05 - 2.13 (m, 1 H), 2.45 - 2.54 (m, 1 H), 3.82 (br s, 1 H), 4.14 (br s, 1 H), 5.32 (br s, 1 H), 5.88 (br s, 1 H), 7.33 (dd, J = 7.72, 4.89 Hz, 1 H), 7.64 (br d, J = 7.88 Hz, 1 H), 7.85 - 7.92 (m, 1 H), 7.97 (br s, 1

H), 8.45 (dd, *J* = 4.73, 1.26 Hz, 1 H), 8.49 - 8.56 (m, 1 H), 13.08 (br s, 1 H). MS (ES+) *m/z* 266 $[M+H]^+$.

3-Phenyl-4-(1*H*-pyrazolo[3,4-*b*]pyridin-4-yl)morpholine (29)

4-Chloro-1*H*-pyrazolo[3,4-*b*]pyridine (100 mg, 0.65 mmol), 3-phenylmorpholine (128 mg, 0.78 mmol) and triethylamine (108 mL, 0.78 mmol) were dissolved in *N*-methyl-2-pyrrolidone (1 mL). The mixture heated in a microwave reactor at 180 °C for 30 min. After cooling the mixture was diluted with methanol, filtered and purified by preparative RP-HPLC, ammonia buffer to give 30 mg (16%) of the title compound. ^{1}H NMR (500 MHz, DMSO-d_6) δ ppm 3.64 - 3.85 (m, 2 H), 3.90 (br d, *J* = 12.30 Hz, 1 H), 4.05 (td, *J* = 7.88, 3.78 Hz, 2 H), 4.17 - 4.27 (m, 1 H), 5.34 (br s, 1 H), 6.39 (d, *J* = 5.67 Hz, 1 H), 7.15 - 7.25 (m, 1 H), 7.25 - 7.36 (m, 4 H), 8.04 (d, *J* = 5.67 Hz, 1 H), 8.14 (s, 1 H), 13.24 (br s, 1 H). MS (ES+) *m/z* 281 $[M+H]^+$.

4-[2-(1-Methoxy-1-methyl-ethyl)pyrrolidin-1-yl]-1*H*-pyrazolo[3,4-*b*]pyridine acetate salt (30)

4-Chloro-1*H*-pyrazolo[3,4-*b*]pyridine (100 mg, 0.65 mmol), 2-(1-methoxy-1-methyl-ethyl)pyrrolidine (121 mg, 0.85 mmol) and triethylamine (180 mL, 1.3 mmol) were dissolved in *N*-methyl-2-pyrrolidone (1 mL). The mixture was heated in a microwave reactor at 230 °C for 1 h. The reaction mixture was purified by preparative RP-HPLC, acetic acid buffer to give 20 mg (10%) of the title compound. ^{1}H NMR (400 MHz, DMSO-d_6) δ ppm 1.10 (s, 3 H), 1.15 (s, 3 H), 1.75 - 1.90 (m, 2 H), 1.91 (s, 3 H), 2.01 - 2.19 (m, 2 H), 3.09 (s, 3 H), 3.35 (br s, 1 H), 3.52 - 3.77 (m, 1 H), 3.82 - 4.00 (m, 1 H), 4.28 (br d, *J* = 7.92 Hz, 1 H), 6.38 (d, *J* = 6.16 Hz, 1 H), 7.94 (d,

J = 5.72 Hz, 1 H), 8.14 (s, 1 H). MS (ES+) *m/z* 261 $[M+H]^+$.

_N_-ethyl-4-[2-(1-methoxy-1-methyl-ethyl)pyrrolidin-1-yl]-1_H_-pyrrolo[2,3-_b_]pyridine-2-carboxamide (31)

n-Butyllithium (3.2 mL, 2.5 M in hexanes, 7.9 mmol), was added slowly to a solution of diisopropylamine (1.1 mL, 7.9 mmol) in 2-methyltetrahydrofuran (10 mL) at 0 °C. The resulting mixture was stirred at 0 °C for 5 min and was then cooled to -78 °C. A solution of 1-(benzenesulfonyl)-4-chloro-pyrrolo[2,3-*b*]pyridine (1.8 g, 6.2 mmol), in 2-methyltetrahydrofuran (10 mL) was added dropwise. The resulting mixture was stirred at -78 °C for 15 min and was then allowed to warm to room temperature. After stirring at room temperature for 10 min, the reaction mixture was cooled to -78 °C again. Carbon dioxide (from dry ice) was bubbled through the reaction mixture and stirring was continued on the thawing ice bath for 1 h. Saturated aqueous ammonium chloride, water and ethyl acetate were added. The formed precipitate was filtered off and washed with cold 2-propanol. The aqueous phase of the combined filtrate was made acidic by the addition of concentrated hydrochloric acid and left to rest overnight. The formed precipitate was collected by suction filtration, washed with cold 2-propanol and pentane and dried. The two solids were combined to give 1.9 g of 1-(benzenesulfonyl)-4-chloro-pyrrolo[2,3-*b*]pyridine-2-carboxylic acid (MS (ES+) *m/z* 338 $[M+H]^+$). A portion of this material (1.5 g, 4.4 mmol) was dissolved in thionyl chloride (3.68 mL, 51 mmol), and the mixture was heated to 80 °C for 20 min. The reaction mixture was concentrated and the crude product was dissolved in dichloromethane (10 mL). Ethylamine (4.45 mL, 2 M in tetrahydrofuran, 8.9 mmol) was slowly added. The reaction mixture was stirred at room temperature for 30 min and then concentrated under vacuum. Ethanol and water were added to the crude product and the formed

precipitate was isolated by filtration, washed with 2-propanol and pentane and dried to give 800 mg of 4-chloro-*N*-ethyl-1*H*-pyrrolo[2,3-*b*]pyridine-2-carboxamide (MS (ES+) *m/z* 224 $[M+H]^+$). A portion of this material (65 mg, 0.29 mmol), 2-(1-methoxy-1-methyl-ethyl)pyrrolidine (42 mg, 0.29 mmol) and *N*,*N*-diisopropylethylamine (80 µL, 0.45 mmol) were dissolved in *N*-methyl-2-pyrrolidone (1 mL). The mixture was heated in a microwave reactor at 220 °C for 1 h and then at 230 °C for 1 h. The reaction mixture was filtered and then purified by preparative RP-HPLC, ammonia buffer to give 10 mg (7%) of the title compound over several steps from 1-(benzenesulfonyl)-4-chloro-pyrrolo[2,3-*b*]pyridine. ^{1}H-NMR (500 MHz, DMSO-d_6): δ ppm 1.08 (s, 3 H), 1.12 - 1.18 (m, 6 H), 1.88 (br s, 2 H), 2.08 (br d, 2 H), 3.12 (s, 3 H), 3.25 - 3.32 (m, 2 H), 3.74 - 3.83 (m, 1 H), 3.86 - 4.01 (m, 1 H), 4.32 (br d, *J* = 7.25 Hz, 1 H), 6.44 (d, *J* = 6.31 Hz, 1 H), 7.33 (s, 1 H), 7.84 (d, *J* = 5.67 Hz, 1 H), 8.27 (br t, *J* = 5.36 Hz, 1 H), 11.53 (br s, 1 H). MS (ES+) *m/z* 331 $[M+H]^+$.

_N_-ethyl-4-[(3_S_)-3-methylmorpholin-4-yl]-1_H_-pyrrolo[2,3-_b_]pyridine-2-carboxamide acetic acid salt (32)

4-Chloro-*N*-ethyl-1*H*-pyrrolo[2,3-*b*]pyridine-2-carboxamide (100 mg, 0.45 mmol), (3*S*)-3-methylmorpholine (59 mg, 0.58 mmol) and triethylamine (0.12 mL, 0.89 mmol) were dissolved in *N*-methyl-2-pyrrolidone (1 mL). The mixture was heated in a microwave reactor at 220 °C for 1 h. The reaction mixture was filtered and then purified in two steps by preparative RP-HPLC, ammonia buffer followed by preparative RP-HPLC, acetic acid buffer to give 5 mg (3%) of the title compound over several steps from 1-(benzenesulfonyl)-4-chloro-pyrrolo[2,3-*b*]pyridine. ^{1}H-NMR (400 MHz, Methanol-d_4): δ ppm 1.24 - 1.33 (m, 6 H), 1.98 (s, 9 H), 3.37 - 3.51 (m, 2 H), 3.54 - 3.64 (m, 2 H), 3.71 - 3.79 (m, 1 H), 3.82 (br d, *J* = 11.44 Hz, 1 H), 3.94 (dd, *J* =

11.44, 2.64 Hz, 1 H), 4.05 (br d, *J* = 11.44 Hz, 1 H), 4.40 (br d, *J* = 5.72 Hz, 1 H), 6.53 (d, *J* = 5.72 Hz, 1 H), 7.33 (s, 1 H), 8.03 (d, *J* = 5.72 Hz, 1 H). MS (ES+) *m/z* 289 $[M+H]^+$. ^{13}C-NMR (101 MHz, DMSO- d_6) d ppm 12.654, 14.966, 33.660, 42.688, 50.418, 66.241, 70.599, 101.601, 101.996, 109.18, 128.800, 146.211, 150.253, 150.826, 160.434.

_N_-ethyl-4-(3-phenylmorpholin-4-yl)-1_H_-pyrrolo[2,3-_b_]pyridine-2-carboxamide (33)

4-Chloro-*N*-ethyl-1*H*-pyrrolo[2,3-*b*]pyridine-2-carboxamide (100 mg, 0.45 mmol), 3-phenylmorpholine (95 mg, 0.58 mmol) and triethylamine (0.12 mL, 0.89 mmol), were dissolved in *N*-methyl-2-pyrrolidone (1 mL). The mixture was heated in a microwave reactor at 220 °C for 1 h and at 230 °C for 1 h. The reaction mixture was filtered and then purified by preparative RP-HPLC, ammonia buffer to give 5 mg (2%) of the title compound over several steps from 1-(benzenesulfonyl)-4-chloro-pyrrolo[2,3-*b*]pyridine. ^{1}H-NMR (400 MHz, DMSO-d_6): δ ppm 1.16 (t, *J* = 7.26 Hz, 3 H), 3.26 - 3.32 (m, 2 H), 3.36 - 3.43 (m, 1 H), 3.74 (dt, *J* = 12.43, 3.69 Hz, 1 H), 3.81 - 4.07 (m, 4 H), 4.99 (br s, 1 H), 6.36 (d, *J* = 5.72 Hz, 1 H), 7.16 - 7.44 (m, 6 H), 7.92 (d, *J* = 5.72 Hz, 1 H), 8.39 (br t, *J* = 5.28 Hz, 1 H), 11.62 (br s, 1 H). MS (ES+) *m/z* 351 $[M+H]^+$.

4-(3-cyclopropylmorpholin-4-yl)-_N_-ethyl-1_H_-pyrrolo[2,3-_b_]pyridine-2-carboxamide (34)

4-Chloro-*N*-ethyl-1*H*-pyrrolo[2,3-*b*]pyridine-2-carboxamide (120 mg, 0.54 mmol), 3-cyclopropylmorpholine (273 mg, 2.2 mmol) and *N*,*N*-diisopropylethylamine (0.37 mL, 2.2 mmol) were mixed in pyridine (0.5 mL) and heated in a microwave reactor at 230 °C for 4 h. Methanol was added and the reaction mixture was filtered and then purified in two steps by

preparative RP-HPLC, acetic acid buffer followed by preparative RP-HPLC, ammonia buffer to give 15 mg (6%) of the title compound over several steps from 1-(benzenesulfonyl)-4-chloro-pyrrolo[2,3-*b*]pyridine. ^{1}H-NMR (500 MHz, DMSO-d_6): δ ppm -0.26 - -0.19 (m, 1 H), 0.12 - 0.23 (m, 2 H), 0.33 - 0.41 (m, 1 H), 1.15 (t, *J* = 7.25 Hz, 3 H), 1.43 - 1.51 (m, 1 H), 3.28 - 3.33 (m, 2 H), 3.34 - 3.38 (m, 1 H), 3.55 (br d, 1 H), 3.61 - 3.66 (m, 2 H), 3.84 (dd, *J* = 11.03, 2.84 Hz, 1 H), 3.90 - 3.95 (m, 1 H), 3.98 - 4.03 (m, 1 H), 6.46 (d, *J* = 5.36 Hz, 1 H), 7.14 (s, 1 H), 8.02 (d, *J* = 5.36 Hz, 1 H), 8.30 (t, *J* = 5.52 Hz, 1 H), 11.58 (br s, 1 H). MS (ES+) *m/z* 315 $[M+H]^+$.

_N_-ethyl-1-methyl-4-[(3*S*)-3-methylmorpholin-4-yl]-1*H*-pyrrolo[2,3-b]pyridine-2-carboxamide (35)

N-ethyl-4-[(3*S*)-3-methylmorpholin-4-yl]-1*H*-pyrrolo[2,3-*b*]pyridine-2-carboxamide (68 mg, 0.24 mmol) was dissolved in tetrahydrofuran (2 mL) and cooled to 0 °C. Sodium hydride (60%) (9.4 mg, 0.24 mmol) was added, followed by iodomethane (15 µl, 0.24 mmol). After stirring for 10 min at 0 °C, water was added slowly. The aqueous phase was extracted three times with ethyl acetate. The combined organic phases were dried and separated via chromatography to obtain 51 mg (68 %) of the title compound. ¹H-NMR (400 MHz, DMSO-d6) δ [ppm]: 1.11 (t, *J* = 7.09 Hz, 3H), 1.26 (d, *J* = 6.84 Hz, 3H), 3.22 - 3.31 (m, 2H), 3.42 - 3.61 (m, 2H), 3.64 - 3.79 (m, 2H), 3.97 (m, 5H), 4.45 - 4.60 (m, 1H), 6.40 (d, *J* = 7.35 Hz, 1H), 7.10 (s, 1H), 7.81 (t, *J* = 6.08 Hz, 1H), 7.86 (d, *J* = 7.10 Hz, 1H). MS (ES+) *m/z* 303 $[M+H]^+$. ^{13}C-NMR (101 MHz, DMSO- d_6): d ppm 14.070, 15.447, 33.092, 38.213, 42.390, 49.996, 66.162, 70.302, 95.852, 103.154, 111.719, 135.521, 141.779, 147.527, 152.375, 164.280.

ASSOCIATED CONTENT

Supporting Information.

The following files are available free of charge:

Table of SMILES and data for all compounds (csv)

Selectivity data of **10** and **24** in a 97-membered kinome panel (csv)

Selectivity data of **24** in a 215-membered ATP-ase panel (xlsx)

Selectivity data of **32** (BAY-707) and **35** (BAY-604) in a 20-membered NudiX panel (csv)

Data collection and refinement statistics, data used for computational modeling, methods for NudiX selectivity assessment (PDF)

AUTHOR INFORMATION

Corresponding Author

*(Jenny Viklund) jenny.viklund@sprintbioscience.com, jenny.viklund@gmail.com

Present Addresses

§Fredrik Rahm, AWApatent AB, Jakobsbergsgatan 36, 111 44 Stockholm

‡Kenth Hallberg, SARomics Biostructures, Medicon Village, 223 81 Lund

Author Contributions

F.R. Sprint Bioscience project coordinator, F.R., J.V, R.F, T.G, J.L, M.E., A.G., J.G., M.B. medicinal chemistry. J.V, L.B.P. computational chemistry. L.T., K.H., A.T. crystallography. U.E, C.S. Protein Science and screening. M.A. target selection. M.G. pharmacology, Bayer project coordinator. O.F., L.D.S., I.P., P.S., K.V.M.H. expression and purification of Nudix selectivity panel proteins and TSA measurements. All authors have given approval to the final version of the manuscript.

Notes

The authors declare no competing financial interest.

ACKNOWLEDGMENT

We acknowledge the European Synchrotron Radiation Facility for provision of synchrotron radiation facilities and the staff of beamlines ID23-1 and ID29 for their support. We also thank Santiago Parpal for support in proof-reading and preparing the manuscript. The SGC is a registered charity (number 1097737) that receives funds from AbbVie, Bayer Pharma AG, Boehringer Ingelheim, Canada Foundation for Innovation, Eshelman Institute for Innovation, Genome Canada, Innovative Medicines Initiative (EU/EFPIA) [ULTRA-DD grant no. 115766], Janssen, Merck KGaA Darmstadt Germany, MSD, Novartis Pharma AG, Ontario Ministry of Economic Development and Innovation, Pfizer, São Paulo Research Foundation-FAPESP, Takeda, and Wellcome [106169/ZZ14/Z].

ABBREVIATIONS

ITC, Isothermal titration calorimetry; NUDIX, NUcleoside DIphosphate linked to another moiety X; MTH1, MutT Homolog1; TSA, Thermal Shift Assay; CETSA, Cellular Thermal Shift Assay; HAC, Heavy Atom Count; PLS, partial-least-squares; DFT, density functional theory

Accession Codes in the PDB for human MTH1 with bound ligands: Compound **1 (**6F20), Compound **7 (**6F1X), Compound **16** (6F23) and Compound **29** (6F22). Authors will release the atomic coordinates and experimental data upon article publication.

REFERENCES

(1) Ellermann, M.; Eheim, A.; Rahm, F.; Viklund, J.; Guenther, J.; Andersson, M.; Ericsson, U.; Forsblom, R.; Ginman, T.; Lindström, J.; Silvander, C.; Trésaugues, L.; Giese, A.; Bunse, S.; Neuhaus, R.; Weiske, J.; Quanz, M.; Glasauer, A.; Nowak-Reppel, K.; Bader, B.; Irlbacher, H.; Meyer, H.; Queisser, N.; Bauser, M.; Haegebarth, A.; Gorjánácz, M. Novel Class of Potent and Cellularly Active Inhibitors Devalidates MTH1 as Broad-Spectrum Cancer Target. *ACS Chem. Biol.* **2017**, *12* (8), 1986–1992.

(2) Liou, M.-Y.; Storz, P. *Reactive Oxygen Species in Cancer*; 2010; Vol. 44.

(3) Klaunig, J. E.; Kamendulis, L. M.; Hocevar, B. A. Oxidative Stress and Oxidative Damage in Carcinogenesis. *Toxicol. Pathol.* **2010**, *38* (1), 96–109.

(4) Gorrini, C.; Harris, I. S.; Mak, T. W. Modulation of Oxidative Stress as an Anticancer Strategy. *Nat. Rev. Drug Discov.* **2013**, *12* (12), 931–947.

(5) Haghdoost, S.; Sjölander, L.; Czene, S.; Harms-Ringdahl, M. The Nucleotide Pool Is a Significant Target for Oxidative Stress. *Free Radic. Biol. Med.* **2006**, *41* (4), 620–626.

(6) Pavlov, Y. I.; Minnick, D. T.; Izuta, S.; Kunkel, T. A. DNA Replication Fidelity with 8-Oxodeoxyguanosine Triphosphate. *Biochemistry* **1994**, *33* (15), 4695–4701.

(7) Bessman, M. J.; Frick, D. N.; O'Handley, S. F. The MutT Proteins or "Nudix" Hydrolases, a Family of Versatile, Widely Distributed, "housecleaning" Enzymes. *J. Biol. Chem.* **1996**, *271* (41), 25059–25062.

(8) Gad, H.; Koolmeister, T.; Jemth, A.-S.; Eshtad, S.; Jacques, S. a; Ström, C. E.; Svensson, L. M.; Schultz, N.; Lundbäck, T.; Einarsdottir, B. O.; Saleh, A.; Göktürk, C.; Baranczewski, P.; Svensson, R.; Berntsson, R. P.; Gustafsson, R.; Strömberg, K.; Sanjiv, K.; Jacques-Cordonnier, M.-C.; Desroses, M.; Gustavsson, A.-L.; Olofsson, R.; Johansson, F.; Homan, E. J.; Loseva, O.; Bräutigam, L.; Johansson, L.; Höglund, A.; Hagenkort, A.; Pham, T.; Altun, M.; Gaugaz, F. Z.; Vikingsson, S.; Evers, B.; Henriksson, M.; Vallin, K. S. a; Wallner, O. a; Hammarström, L. G. J.; Wiita, E.; Almlöf, I.; Kalderén, C.; Axelsson, H.; Djureinovic, T.; Puigvert, J. C.; Häggblad, M.; Jeppsson, F.; Martens, U.; Lundin, C.; Lundgren, B.; Granelli, I.; Jensen, A. J.; Artursson, P.; Nilsson, J. a; Stenmark, P.; Scobie, M.; Berglund, U. W.; Helleday, T. MTH1 Inhibition Eradicates Cancer by Preventing Sanitation of the dNTP Pool. *Nature* **2014**, *508* (7495), 215–221.

(9) Nakabeppu, Y.; Kajitani, K.; Sakamoto, K.; Yamaguchi, H.; Tsuchimoto, D. MTH1, an Oxidized Purine Nucleoside Triphosphatase, Prevents the Cytotoxicity and Neurotoxicity of Oxidized Purine Nucleotides. *DNA Repair (Amst).* **2006**, *5* (7), 761–772.

(10) Rai, P.; Young, J. J.; Burton, D. G. A.; Giribaldi, M. G.; Onder, T. T.; Weinberg, R. A. Enhanced Elimination of Oxidized Guanine Nucleotides Inhibits Oncogenic RAS-Induced DNA Damage and Premature Senescence. *Oncogene* **2011**, *30* (12), 1489–1496.

(11) Patel, a; Burton, D. G. a; Halvorsen, K.; Balkan, W.; Reiner, T.; Perez-Stable, C.; Cohen, a; Munoz, a; Giribaldi, M. G.; Singh, S.; Robbins, D. J.; Nguyen, D. M.; Rai, P. MutT Homolog 1 (MTH1) Maintains Multiple KRAS-Driven pro-Malignant Pathways. *Oncogene* **2014**, *1* (January), 1–11.

(12) Huber, K. V. M.; Salah, E.; Radic, B.; Gridling, M.; Elkins, J. M.; Stukalov, A.; Jemth, A.-S.; Göktürk, C.; Sanjiv, K.; Strömberg, K.; Pham, T.; Berglund, U. W.; Colinge, J.; Bennett, K. L.; Loizou, J. I.; Helleday, T.; Knapp, S.; Superti-Furga, G. Stereospecific Targeting of MTH1 by (S)-Crizotinib as an Anticancer Strategy. *Nature* **2014**, *508* (7495), 222–227.

(13) Berman, H. M.; Battistuz, T.; Bhat, T. N.; Bluhm, W. F.; Bourne, P. E.; Burkhardt, K.; Feng, Z.; Gilliland, G. L.; Iype, L.; Jain, S.; Fagan, P.; Marvin, J.; Padilla, D.; Ravichandran, V.; Schneider, B.; Thanki, N.; Weissig, H.; Westbrook, J. D.; Zardecki, C. The Protein Data Bank. *Acta Crystallogr. D. Biol. Crystallogr.* **2002**, *58* (Pt 6 No 1), 899–907.

(14) Tresaugues, L.; Siponen, M. .; Arrowsmith, C. .; Berglund, H.; Bountra, C.; Collins, R.; Edwards, A. .; Ekblad, T.; Flodin, S.; Flores, A.; Graslund, S.; Hammarstrom, M.; Johansson, I.; Karlberg, T.; Kol, S.; Kotenyova, T.; Kouznetsova, E.; Moche, M.; Nyman, T.; Persson, C.; Schuler, H.; Schutz, P.; Thorsell, A. .; Van Der Berg, S.; Wahlberg, E.; Weigelt, J.; Welin, M.; Nordlund, P. Crystal Structure of Human 8-Oxo-dGTPase (MTH1). Deposited in PDB as 3Q93, **2011**

(15) Waz, S.; Nakamura, T.; Hirata, K.; Koga-Ogawa, Y.; Chirifu, M.; Arimori, T.; Tamada, T.; Ikemizu, S.; Ô, Y. N.; Yamagata, Y. Structural and Kinetic Studies of the Human Nudix Hydrolase MTH1 Reveal the Mechanism for Its Broad Substrate Specificity. *J. Biol. Chem.* **2017**, *292* (7), 2785–2794.

(16) Nissink, J. W. M.; Bista, M.; Breed, J.; Carter, N.; Embrey, K.; Read, J.; Winter-Holt, J. J. MTH1 Substrate Recognition—An Example of Specific Promiscuity. *PLoS One* **2016**, *11* (3), e0151154.

(17) Kettle, J. G.; Alwan, H.; Bista, M.; Breed, J.; Davies, N. L.; Eckersley, K.; Fillery, S.; Foote, K. M.; Goodwin, L.; Jones, D. R.; Käck, H.; Lau, A.; Nissink, J. W. M.; Read, J.; Scott, J. S.; Taylor, B.; Walker, G.; Wissler, L.; Wylot, M. Potent and Selective Inhibitors of MTH1 Probe Its Role in Cancer Cell Survival. *J. Med. Chem.* **2016**, *59* (6), 2346–2361.

(18) Svensson, L. M.; Jemth, A. S.; Desroses, M.; Loseva, O.; Helleday, T.; Högbom, M.; Stenmark, P. Crystal Structure of Human MTH1 and the 8-Oxo-dGMP Product Complex. *FEBS Lett.* **2011**, *585* (16), 2617–2621.

(19) Petrocchi, A.; Leo, E.; Reyna, N. J.; Hamilton, M. M.; Shi, X.; Parker, C. A.; Mseeh, F.; Bardenhagen, J. P.; Leonard, P.; Cross, J. B.; Huang, S.; Jiang, Y.; Cardozo, M.; Draetta, G.; Marszalek, J. R.; Toniatti, C.; Jones, P.; Lewis, R. T. Identification of Potent and Selective MTH1 Inhibitors. *Bioorg. Med. Chem. Lett.* **2016**, *26* (6), 1503–1507.

(20) Kawamura, T.; Kawatani, M.; Muroi, M.; Kondoh, Y.; Futamura, Y.; Aono, H.; Tanaka, M.; Honda, K.; Osada, H. Proteomic Profiling of Small-Molecule Inhibitors Reveals Dispensability of MTH1 for Cancer Cell Survival. *Sci. Rep.* **2016**, *6* (May), 1–9.

(21) Kaelin, W. G. Common Pitfalls in Preclinical Cancer Target Validation. *Nat. Rev. Cancer* **2017**, *17* (7), 441–450.

(22) Samaranayake, G. J.; Huynh, M.; Rai, P. MTH1 as a Chemotherapeutic Target: The Elephant in the Room. *Cancers (Basel).* **2017**, *9* (5), 47.

(23) Arrowsmith, C. H.; Audia, J. E.; Austin, C.; Baell, J.; Bennett, J.; Blagg, J.; Bountra, C.; Brennan, P. E.; Brown, P. J.; Bunnage, M. E.; Buser-Doepner, C.; Campbell, R. M.; Carter, A. J.; Cohen, P.; Copeland, R. A.; Cravatt, B.; Dahlin, J. L.; Dhanak, D.; Edwards, A. M.; Frye, S. V.; Gray, N.; Grimshaw, C. E.; Hepworth, D.; Howe, T.; Huber, K. V. M.; Jin, J.; Knapp, S.; Kotz, J. D.; Kruger, R. G.; Lowe, D.; Mader, M. M.; Marsden, B.; Mueller-Fahrnow, A.; Müller, S.; O'Hagan, R. C.; Overington, J. P.; Owen, D. R.; Rosenberg, S. H.; Roth, B.; Ross, R.; Schapira, M.; Schreiber, S. L.; Shoichet, B.; Sundström, M.; Superti-Furga, G.; Taunton, J.; Toledo-Sherman, L.; Walpole, C.; Walters, M. A.; Willson, T. M.; Workman, P.; Young, R. N.; Zuercher, W. J. The Promise and Peril of Chemical Probes. *Nat. Chem. Biol* **2015**, *11* (8), 536–541.

(24) Blagg, J.; Workman, P. Choose and Use Your Chemical Probe Wisely to Explore Cancer Biology. *Cancer Cell* **2017**, *32* (1), 9–25.

(25) Miyaura, N.; Yamada, K.; Suzuki, A. A New Stereospecific Cross-Coupling by the Palladium-Catalyzed Reaction of 1-Alkenylboranes with 1-Alkenyl or 1-Alkynyl Halides. *Tetrahedron Lett.* **1979**, No. 36, 3437–3440.

(26) Guram, A. S.; Rennels, R. A.; Buchwald, S. L. A Simple Catalytic Method for the Conversion of Aryl Bromides to Arylamines. *Angew. Chemie Int. Ed. English* **1995**, *34* (12),

1348–1350.

(27) Louie, J.; Hartwig, J. F. Palladium-Catalyzed Synthesis of Arylamines from Aryl Halides. Mechanistic Studies Lead to Coupling in the Absence of Tin Reagents. *Tetrahedron Lett.* **1995**, *36* (21), 3609–3612.

(28) Edfeldt, F. N. B.; Folmer, R. H. A.; Breeze, A. L. Fragment Screening to Predict Druggability (Ligandability) and Lead Discovery Success. *Drug Discov. Today* **2011**, *16* (7–8), 284–287.

(29) Meanwell, N. A. Improving Drug Candidates by Design: A Focus on Physicochemical Properties As a Means of Improving Compound Disposition and Safety. *Chem. Res. Toxicol.* **2011**, *24* (9), 1420–1456.

(30) Hopkins, A. L.; Groom, C. R.; Alex, A. Ligand Efficiency: A Useful Metric for Lead Selection. *Drug Discov. Today* **2004**, *9* (10), 430–431.

(31) Hann, M. M.; Keserü, G. M. Finding the Sweet Spot: The Role of Nature and Nurture in Medicinal Chemistry. *Nat. Rev. Drug Discov.* **2012**, *11* (5), 355–365.

(32) Mérour, J.-Y.; Buron, F.; Plé, K.; Bonnet, P.; Routier, S. The Azaindole Framework in the Design of Kinase Inhibitors. *Molecules* **2014**, *19* (12), 19935–19979.

(33) Lovering, F.; Bikker, J.; Humblet, C. Escape from Flatland: Increasing Saturation as an Approach to Improving Clinical Success. *J. Med. Chem.* **2009**, *52* (21), 6752–6756.

(34) Young, R. J.; Green, D. V. S.; Luscombe, C. N.; Hill, A. P. Getting Physical in Drug Discovery II: The Impact of Chromatographic Hydrophobicity Measurements and

Aromaticity. *Drug Discov. Today* **2011**, *16* (17–18), 822–830.

(35) Winiwarter, S.; Ax, F.; Lennernäs, H.; Hallberg, A.; Pettersson, C.; Karlén, A. Hydrogen Bonding Descriptors in the Prediction of Human in Vivo Intestinal Permeability. *J. Mol. Graph. Model.* **2003**, *21* (4), 273–287.

(36) Leeson, P. D.; Young, R. J. Molecular Property Design: Does Everyone Get It? *ACS Med. Chem. Lett.* **2015**, *6* (7), 722–725.

(37) Hann, M. M. Molecular Obesity, Potency and Other Addictions in Drug Discovery. *Med. Chem. Commun.*, 2011, 2, 349-355.

(38) Testa, B.; Krämer, S. D. The Biochemistry of Drug Metabolism – An Introduction. *Chem. Biodivers. (Wiley)* **2007**, *4* (9), 2031–2122.

(39) Mancera, R. L. Molecular Modeling of Hydration in Drug Design. *Curr. Opin. Drug Discov. Devel.* **2007**, *10* (3), 275–280.

(40) Wang, L.; Berne, B. J.; Friesner, R. A. Ligand Binding to Protein-Binding Pockets with Wet and Dry Regions. *Proc. Natl. Acad. Sci.* **2011**, *108* (4), 1326–1330.

(41) Molina, D. M.; Jafari, R.; Ignatushchenko, M.; Seki, T.; Larsson, E. A.; Dan, C.; Sreekumar, L.; Cao, Y.; Nordlund, P. Monitoring Drug Target Engagement in Cells and Tissues Using the Cellular Thermal Shift Assay. *Science.* **2013**, *341* (6141), 84–87.

(42) Wang, L.; Wu, Y.; Deng, Y.; Kim, B.; Pierce, L.; Krilov, G.; Lupyan, D.; Robinson, S.; Dahlgren, M. K.; Greenwood, J.; Romero, D. L.; Masse, C.; Knight, J. L.; Steinbrecher, T.; Beuming, T.; Damm, W.; Harder, E.; Sherman, W.; Brewer, M.; Wester, R.; Murcko, M.;

Frye, L.; Farid, R.; Lin, T.; Mobley, D. L.; Jorgensen, W. L.; Berne, B. J.; Friesner, R. A.; Abel, R. Accurate and Reliable Prediction of Relative Ligand Binding Potency in Prospective Drug Discovery by Way of a Modern Free-Energy Calculation Protocol and Force Field. *J. Am. Chem. Soc.* **2015**, *137* (7), 2695–2703.

(43) Rudling, A.; Gustafsson, R.; Almlöf, I.; Homan, E.; Scobie, M.; Warpman Berglund, U.; Helleday, T.; Stenmark, P.; Carlsson, J. Fragment-Based Discovery and Optimization of Enzyme Inhibitors by Docking of Commercial Chemical Space. *J. Med. Chem.* **2017**, *60* (19), 8160–8169.

(44) DeLano, W. L. Unraveling Hot Spots in Binding Interfaces: Progress and Challenges. *Curr. Opin. Struct. Biol.* **2002**, *12* (1), 14–20.

(45) Ciulli, A.; Williams, G.; Smith, A. G.; Blundell, T. L.; Abell, C. Probing Hot Spots at Protein-Ligand Binding Sites: A Fragment-Based Approach Using Biophysical Methods. *J. Med. Chem.* **2006**, *49* (16), 4992–5000.

(46) Roos, K.; Viklund, J.; Meuller, J.; Kaspersson, K.; Svensson, M. Potency Prediction of β-Secretase (BACE-1) Inhibitors Using Density Functional Methods. *J. Chem. Inf. Model.* **2014**, *54* (3), 818–825.

(47) Lee, J. B.; Zgair, A.; Taha, D. A.; Zang, X.; Kagan, L.; Kim, T. H.; Kim, M. G.; Yun, H.-Y.; Fischer, P. M.; Gershkovich, P. Quantitative Analysis of Lab-to-Lab Variability in Caco-2 Permeability Assays. *Eur. J. Pharm. Biopharm.* **2017**, *114*, 38–42.

(48) Kabsch, W. XDS. *Acta Crystallogr. D. Biol. Crystallogr.* **2010**, *66* (Pt 2), 125–132.

(49) Winn, M. D.; Ballard, C. C.; Cowtan, K. D.; Dodson, E. J.; Emsley, P.; Evans, P. R.; Keegan, R. M.; Krissinel, E. B.; Leslie, A. G. W.; Mccoy, A.; Mcnicholas, S. J.; Murshudov, G. N.; Pannu, N. S.; Potterton, E. A.; Powell, H. R.; Read, R. J.; Vagin, A.; Wilson, K. S. Overview of the CCP4 Suite and Current Developments. *Acta Cryst* **2011**, *67*, 235–242.

(50) McCoy, A. J.; Grosse-Kunstleve, R. W.; Adams, P. D.; Winn, M. D.; Storoni, L. C.; Read, R. J. Phaser Crystallographic Software. *J. Appl. Crystallogr.* **2007**, *40* (Pt 4), 658–674.

(51) Emsley, P.; Lohkamp, B.; Scott, W. G.; Cowtan, K. Features and Development of Coot. *Acta Cryst* **2010**, *66*, 486–501.

(52) Murshudov, G. N.; Vagin, A. A.; Dodson, E. J. Refinement of Macromolecular Structures by the Maximum-Likelihood Method. *Acta Crystallogr. D. Biol. Crystallogr.* **1997**, *53* (Pt 3), 240–255.

(53) Painter, J.; Merritt, E. A. TLSMD Web Server for the Generation of Multi-Group TLS Models. *J. Appl. Crystallogr.* **2006**, *39* (1), 109–111.

(54) Gad, H.; Koolmeister, T.; Jemth, A. S.; Eshtad, S.; Jacques, S. A.; Ström, C. E.; Svensson, L. M.; Schultz, N.; Lundbäck, T.; Einarsdottir, B. O.; Saleh, A.; Göktürk, C.; Baranczewski, P.; Svensson, R.; Berntsson, R. P. A.; Gustafsson, R.; Strömberg, K.; Sanjiv, K.; Jacques-Cordonnier, M. C.; Desroses, M.; Gustavsson, A. L.; Olofsson, R.; Johansson, F.; Homan, E. J.; Loseva, O.; Bräutigam, L.; Johansson, L.; Höglund, A.; Hagenkort, A.; Pham, T.; Altun, M.; Gaugaz, F. Z.; Vikingsson, S.; Evers, B.; Henriksson, M.; Vallin, K. S. A.; Wallner, O. A.; Hammarström, L. G. J.; Wiita, E.; Almlöf, I.; Kalderén, C.; Axelsson, H.; Djureinovic, T.; Puigvert, J. C.; Häggblad, M.; Jeppsson, F.; Martens, U.; Lundin, C.;

Lundgren, B.; Granelli, I.; Jensen, A. J.; Artursson, P.; Nilsson, J. A.; Stenmark, P.; Scobie, M.; Berglund, U. W.; Helleday, T. MTH1 Inhibition Eradicates Cancer by Preventing Sanitation of the dNTP Pool. *Nature* **2014**, *508* (7495), 215–221.

(55) Houston, J. B. Utility of in Vitro Drug Metabolism Data in Predicting in Vivo Metabolic Clearance. *Biochem. Pharmacol.* **1994**, *47* (9), 1469–1479.

(56) Baranczewski, P.; Stańczak, A.; Sundberg, K.; Svensson, R.; Wallin, A.; Jansson, J.; Garberg, P.; Postlind, H. Introduction to in Vitro Estimation of Metabolic Stability and Drug Interactions of New Chemical Entities in Drug Discovery and Development. *Pharmacol. Rep.* **2006** *58* (4), 453–472.

Table of Contents Graphic